ONLINE MONITORING OF DIELECTRIC DISSIPATION FACTOR

A dissertation
submitted in partial fulfillment of the requirements
for the degree of

Master of Technology

by

Dayashankar Dubey

(Roll No. 02307402)

under the supervision of

Prof. P. C. Pandey

Department of Electrical Engineering
Indian Institute of Technology, Bombay

July 2005

Dayashankar Dubey / Prof. P. C. Pandey (supervisor): “Online monitoring of dielectric dissipation factor”, *M.Tech. dissertation*, Dept. of Electrical Engineering, Indian Institute of Technology, Bombay, July 2005.

ABSTRACT

A technique for online monitoring of dissipation factor in the range of 500–5000×10^{-5}, with a precision better than 5×10^{-5} is investigated using numerical simulation, a low voltage setup with loss angle simulator circuit, and a high voltage setup with test objects operating at 1 kV. The technique is based on synchronous detection method of phase measurement. The dissipation factor is obtained by processing the simultaneously sampled signals corresponding to voltage and current, and involves dividing the low pass filtered product of voltage and current signals by the RMS values of the two signals. The measurement update rate depends on the response time of the low pass filters. It is shown that the desired precision can be obtained using asynchronous sampling with (a) sampling rate much larger than the power line frequency, giving high update rate, and (b) sampling rate lower than the power line frequency and processing the aliased periodic waveforms retaining the original phase relationship. The second method can be used for low cost instrumentation for condition monitoring applications with low measurement update rate.

ACKNOWLEDGEMENTS

I would like to express my deepest gratitude and sincere thank to my research supervisor Dr. P. C. Pandey for his valuable guidance, support, and encouragement throughout the course of this project and report preparation.

I sincerely thank Dr. S. R. Kannan of M/s Crompton Greaves for encouraging me and extending all the support for undertaking my studies at IIT Bombay. I would like to thank my senior colleagues Mr. Venkatasami and Mr. Yargole for extending support and help in carrying out experiments in the High Voltage Lab of M/s Crompton Greaves, Mumbai. I also wholeheartedly thank my colleagues Ramakichenan, Sravanthi, and Manoj for helping me, in carrying out experiments there. I am especially thankful to my two other colleagues M. D. Pereira and Raju Patange, who helped me in making the low voltage set-up.

I am sincerely thankful to Mr. Vidyadhar Kamble for his guidance in hardware circuitry and laboratory support. I acknowledge the help and support given by my lab colleagues Alice, Milind, Vinod, Sarika, Syrpailyne and Navaneetha for their kind support.

My parents, my sisters and my brothers were very eager to see my project complete successfully. I am ever grateful to them for the motivation and encouragement provided by them through out my research project.

I sincerely thank all my professors of IIT Bombay who taught me different courses that helped me a lot in completing the project successfully.

Dayashankar Dubey

July 2005

CONTENTS

LIST OF SYMBOLS

Symbol	Explanation
δ	Loss angle
ω	Digital frequency
ω_c	Digital cut-off frequency
ω_o	Digital power line frequency
f	Analog frequency
f_c	Analog cut off frequency
f_o	Analog power line frequency
f_s	Sampling rate
L	Number of ADC bits
Δ_q	Quantization step
γ	Normalized cut-off frequency (f_c / f_s)
σ	Standard deviation
φ_m	Phase delay
N	Filter order
n	Samples
t	Time
V	Voltage
V_m	Peak voltage
V_{pp}	peak-to-peak voltage
V_s	Supply voltage
I	Current
I_m	Peak current

LIST OF ABBREVIATIONS

Symbol	Explanation
ADC	Analog-to-digital converter
AGC	Automatic gain control
BPF	Band pass filter
DFT	Discrete Fourier transform
DSO	Digital storage oscilloscope
dB	Decibel
FIR	Finite impulse response
FFT	Fast Fourier transform
Hz	Hertz
I/V	Current to Voltage
IIR	Infinite impulse response
LPF	Low pass filter
PC	Personal computer
p.s.d.	Power density spectrum
RMS	Root mean square
rad	Radian
rad/sa	Radian/sample
Sa/s	Samples/second
s.d.	Standard deviation

LIST OF FIGURES

LIST OF TABLES

Chapter 1

INTRODUCTION

1.1 Overview

A capacitor with a lossy dielectric can be represented by a capacitor C_p in parallel with a resistor R_p as shown in Fig. 1.1. For sinusoidal voltage $v(t)$ of frequency f,

$$v(t) = V_m \cos 2\pi f t \tag{1.1}$$

Capacitive current component $i_C(t)$ and resistive current component $i_R(t)$ are,

$$i_C(t) = (2\pi f C_p V_m)\cos(2\pi f t + \pi/2) \tag{1.2}$$

$$i_R(t) = (V_m / R_p)\cos 2\pi f t \tag{1.3}$$

The net current $i(t)$ is given as,

$$i(t) = \sqrt{f^2 C_p^2 + R_p^{-2}}\, V_m \cos(2\pi f t + \pi/2 - \delta) \tag{1.4}$$

where,

$$\tan\delta = (2\pi f C_p R_p)^{-1} \tag{1.5}$$

The angle δ is known as the loss angle and tan δ is known as the dissipation factor.

The corresponding RMS values are

$$V = V_m / \sqrt{2} \tag{1.6}$$

$$I_C = 2\pi f C_p V \tag{1.7}$$

$$I_R = V / R_p \tag{1.8}$$

$$I = \sqrt{I_C^2 + I_R^2} \tag{1.9}$$

Therefore, the dissipation factor D = tan δ is given as,

$$\tan\delta = I_R / I_C \tag{1.10}$$

The net current I lags the capacitive current component I_C by loss angle δ, and leads the resistive current component by an angle $\pi/2 - \delta$.

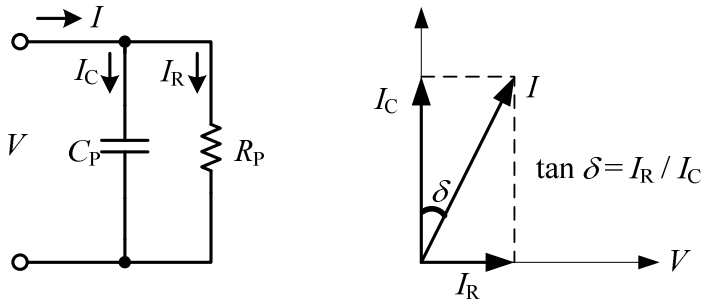

Fig. 1.1 Equivalent parallel RC circuit for a capacitor with lossy dielectric

The capacitor with the lossy dielectric may also be modeled as a capacitor C_s in series with resistor R_s as shown in Fig.1.2. Here the net voltage V lags the voltage across the capacitor V_c by the loss angle δ, and leads the voltage across the resistor by angle $\pi/2 - \delta$. The dissipation factor is given as,

$$\tan \delta = V_R / V_C = 2\pi f \, C_s R_s \tag{1.12}$$

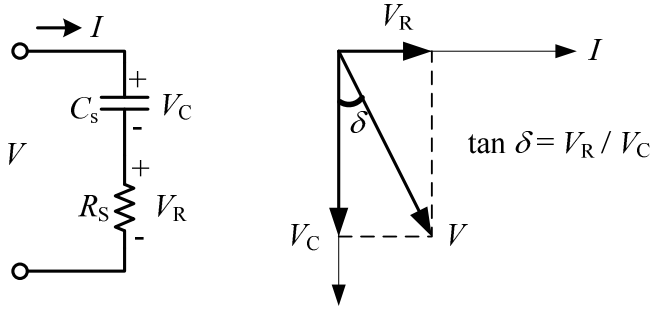

Fig. 1.2 Equivalent series RC circuit for a capacitor with lossy dielectric

High voltage equipment generally involves use of dielectric materials as insulation between conductors, or between conducting parts and the ground. Monitoring of the condition of the insulation is important, because failures of insulation due to ageing and deterioration often involve loss of capital and risk of human injury. When a dielectric is used for insulation in high voltage applications, the loss angle goes on increasing as the

insulation condition deteriorates. Hence measurement of the loss angle or dissipation factor can serve as one of the several techniques for condition monitoring of insulation [1-15]. Offline measurement involves removal of high voltage equipment from the service. Further it is a tedious and time consuming operation. With online monitoring of the dissipation factor, insulation deterioration can be monitored continuously under the actual voltage and temperature conditions, independent of the scheduled offline checks, and this can help in timely detection of insulation failure.

1.2 Project objective

The objective is to develop instrumentation for online measurement of dissipation factor. The work involved numerical simulation of the earlier proposed technique to investigate the associated errors, to test it with a dissipation factor simulator circuit, and finally to develop a signal conditioning circuit to acquire signal from high voltage front end and measure dissipation factor of transformer bushing. It is a continuation of the earlier work done at IIT Bombay [15]. Initially numerical simulation is done to find out the errors contributed by ADC resolution, power line harmonics, and power line frequency fluctuation. Further analysis is done to investigate errors associated with different sampling rates by sampling the signals at two different sampling rates i.e. one higher than the power line frequency and other lower than the power line frequency. A low voltage signal conditioning set-up is made to measure the dissipation factor of transformer bushing rated for 1 kV wherein USB based data acquisition card is used to acquire the signals from the signal conditioning circuit. These acquired signals are processed using MATLAB to compute the dissipation factor.

1.3 Dissertation outline

The second chapter gives literature review of some of the earlier reported techniques. Chapter 3 explains the proposed technique for online dissipation factor measurement along with theoretical error analysis. Chapter 4 explains the numerical simulation used to validate the proposed technique. In Chapter 5, a loss angle simulator circuit along with the results obtained is presented. Experimental hardware setup for dissipation factor measurement of 1 kV bushing and a standard air capacitor of

1000 pF / 2 kV is presented along with the results and discussion in Chapter 6. The last chapter gives the summary and scope for future work.

Chapter 2
DISSIPATION FACTOR MONITORING

In this chapter, a review of the methods of dissipation factor measurement is presented. The techniques for monitoring of dissipation factor can be classified as bridge balancing techniques [3], techniques based on phase measurement [4][10], techniques based on harmonic analysis [5][7][8], techniques based on synchronous detection [6][9], techniques based on decomposition of current signal into orthogonal components [13][16], and technique based on sum current method [11][12]. A number of techniques [17][18][19][20] for phase measurement based on zero-crossing detection are reported in the literature. However, the application of these techniques towards the measurement of dissipation factor has not been reported. The bridge balancing techniques are mostly used for offline measurement while the others techniques are more suitable for online measurement.

2.1 Offline measurement using bridge balancing

A conventional offline technique of monitoring the status of dielectric needs removal of equipment from the service. Two different offline measurement techniques are reported in the literature.

First technique of offline method involves dissipation factor measurement through Schering bridge null detection [3]. This method of measurement is illustrated in Fig. 2.1. Sample dielectric or insulation whose dissipation factor is to be measured is represented by Z_x, where R_p is the resistance representing its dielectric loss component. C_s is a standard air capacitor, while R_v and C_v are variable resistor and capacitor respectively, used for balancing the bridge. Bridge is balanced by successive variation of R_v and C_v until the detector shows null indication.

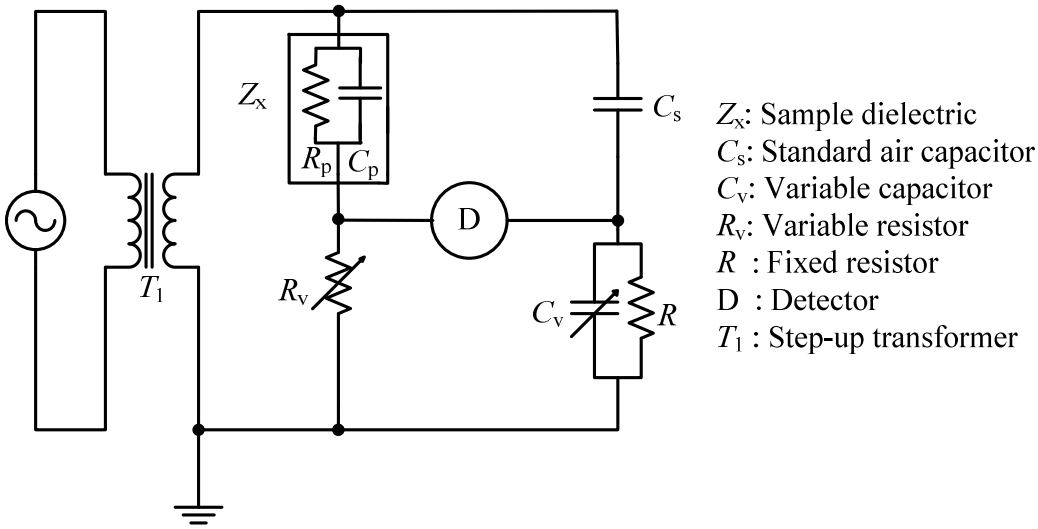

Fig. 2.1 Dissipation factor measurement using Schering bridge (Adapted from [3])

Let Z_1, Z_2, Z_3 and Z_4 represent the impedance of four arms of the Schering bridge shown in Fig. 2.1, where

$Z_1 = R_p \| (1/j\omega C_p),\ \angle Z_1 = \tan^{-1}(\omega C_p R_p)$

$Z_2 = 1/j\omega C_s,\ \angle Z_2 = \pi/2$

$Z_3 = R_v,\ \angle Z_3 = 0$

$Z_4 = R \| (1/j\omega C_v),\ \angle Z_4 = \tan^{-1}(\omega C_v R)$

For bridge to balance

$Z_1 Z_4 = Z_2 Z_3$

i.e., product of magnitude of impedances Z_1 and Z_4 must be equal to product of Z_2 and Z_3

$$|Z_1||Z_4| = |Z_2||Z_3| \tag{2.1}$$

and sum of phase angle of Z_1 and Z_4 must be equal to sum of phase angle of Z_2 and Z_3

$$\angle Z_1 + \angle Z_4 = \angle Z_2 + \angle Z_3 \tag{2.2}$$

Substituting the value of $\angle Z_1$, $\angle Z_2$, $\angle Z_3$ and $\angle Z_4$ in (2.2), we get

$$\tan^{-1}(\omega C_p R_p) + \tan^{-1}(\omega C_v R) = \pi/2$$

which gives,

$$\frac{1}{\omega C_p R_p} = \omega C_v R \tag{2.3}$$

Since the dissipation factor for unknown load Z_x is given as

$$\tan\delta = \omega C_p R_p \tag{2.4}$$

the dissipation factor, under the bridge balance condition is given by

$$\tan\delta = \omega C_v R \tag{2.5}$$

Various instruments based on Schering bridge method are available. These instruments either have automatic or manual bridge balancing. Table 2.1 lists some of the instruments along with the name of manufactures and specification. All these instruments have an internal standard capacitor.

Table 2.1 List of tan δ measuring instruments based on Schering bridge method

Manufacturer	**Model No.**	**Specifications**				
		tan δ range	**Test voltage (kV)**	**Accuracy**	**Resolution**	**Bridge balance**
Doble [21]	M4100	0 to $\pm$2	25-12	$\pm 40\times10^{-5}$	10×10^{-5}	Auto
Haefely [22]	Type 470	Not available	Not available	Not available	Not available	Manual
Tettex [22]	Type 2816	0-9.99	0-12	$\pm$1% rdg* $+10\times10^{-5}$	10×10^{-5}	Auto
Megger [23]	Delta 2000	0-0.09	0-10	$\pm$2% rdg	10×10^{-5}	Auto
Sivananda Electronics [24]	MLS-11DA1	100×10^{-5}-2	0-10	$\pm$1% rdg $\pm 50\times10^{-5}$	10×10^{-5}	Auto
Tinsley [25]	AFP3000 bridge	0-1	0-12	1% rdg $\pm 20\times10^{-5}$	1×10^{-5}	Auto
Scope T&M[26]	FT-12	10×10^{-5}-10	0-12	$\pm$1% rdg	10×10^{-5}	Auto
Eltel [27]	ACTS-12K	0 to $\pm$ infinity	0-12	$\pm$1% rdg $\pm 50\times10^{-5}$	1×10^{-5}	Auto
Lemke Diagnostics [28]	LDV-5/E	10×10^{-5}-100	0-1000	$\pm$1% rdg $\pm 1\times10^{-5}$	0.1×10^{-5}	Auto

* Reading

Technique of offline measurement is based on the operation of cathode ray oscilloscope [3]. It is based on the principle that if the X and Y pairs of plates are applied with an alternating potential difference then the electron beam will trace an ellipse whose area will depend on the phase difference between the alternating voltages applied to the pair of plates. In one method, a potential difference proportional to the applied voltage is applied to one plate of the pair of plates with other plate grounded and another pair of plate excited with a voltage proportional to the integral of current through the dielectric. A record of the ellipse traced out in dissipation factor measurements can be obtained photographically. Another method under this technique is shown in Fig. 2.2, Z_x is the sample dielectric or insulation whose dissipation factor is to be measured. By varying the resistor R_v and capacitor C_v, area of ellipse on CRO is reduced so as to make it a straight vertical line. Values of component corresponding to straight-line on CRO give dissipation factor. This method is inaccurate unless the voltage on C_v is much less than that on C_p. Otherwise an amplifier will be needed between C_v and the Y plates. Information on instruments based on this technique could not be obtained.

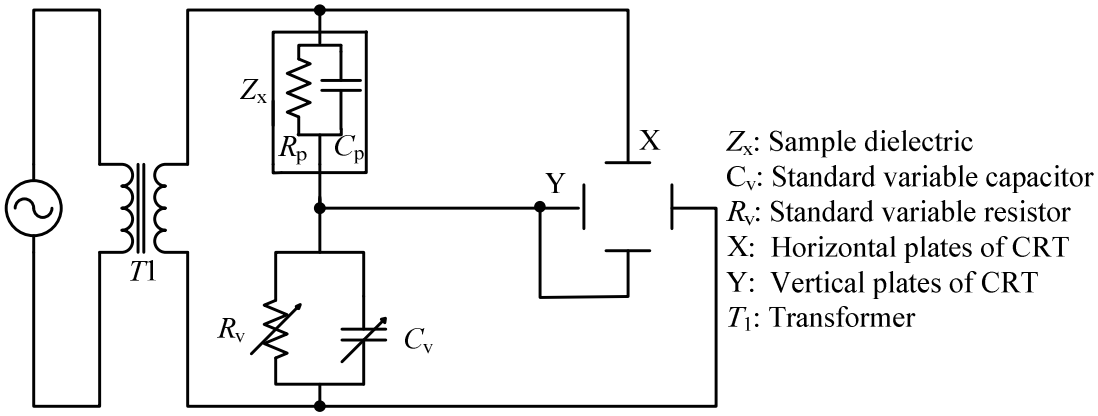

Fig 2.2 CRO technique of dissipation factor measurement (Adapted from [3])

2.2 Online techniques based on phase measurement

Different online techniques have been reported [4-10]. First category includes instrumentation for online monitoring of dissipation factor based on phase measurement. It is essentially acquiring voltage and current signal from the test object and then

performing signal processing on these signals to measure phase difference, the loss angle, or the dissipation factor [4]. Fig. 2.3 shows the general schematic of this arrangement for measuring dissipation factor of high voltage equipment. The dielectric sample or insulation is represented by Z_x, and is connected to high voltage bus, and a voltage divider is used to get the voltage signal. The current through the capacitor is converted into voltage by I/V converter. The two output signals are given to the phase measurement circuit that gives dissipation factor.

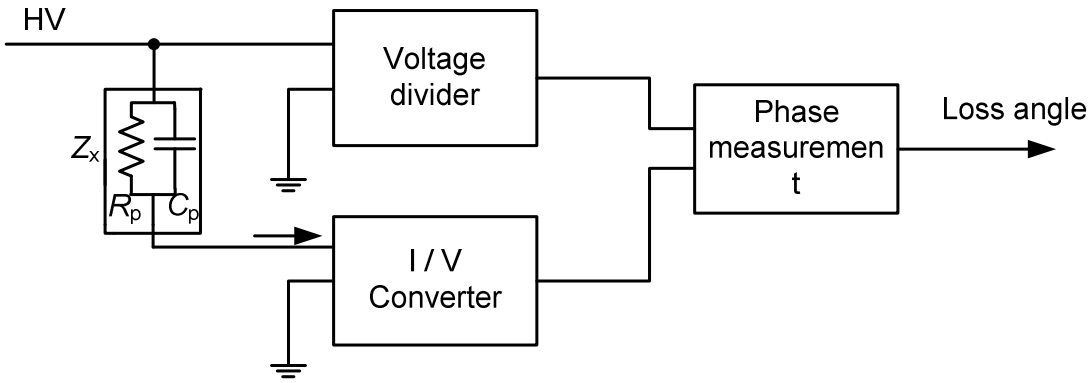

Fig. 2.3 Dissipation factor measurement using phase measurement

A technique of loss angle measurement involves detection phase difference between the zero crossing of current and voltage signal. The reported [10] technique removes the error due to the offset and switching time delays of voltage and current comparators. This is achieved by passing the voltage and current signal through automatic gain amplifier (AGC). The schematic arrangement of this technique to measure the dissipation factor is shown in Fig. 2.4. The current through the dielectric sample is measured as the voltage across standard capacitor connected in series with dielectric sample. The voltage signal is obtained through the capacitor divider connected with test supply. These two signals are then passed through an automatic gain controlled amplifier (AGC). This helps in making the input of voltage of comparator at maximum. The outputs of the current and voltage amplifiers are processed through a harmonic filter to remove any high frequency noise present in the signal. Filtered current and voltage signals are then converted into a square wave using two comparators. The exclusive-OR gate is used to generate a pulse corresponding to the phase difference between the voltage

and current signal. The gate pulses obtained from the exclusive–OR gate is averaged using the low pass filter. If the gate output switches between well defined logic levels 0 volts and V_H volts, then the average output voltage

$$V = V_H \phi / \pi \tag{2.6}$$

where, ϕ is the phase difference. It also includes a digital precedence detector fed from the comparator output that indicates the lead / lag in the phase difference measured.

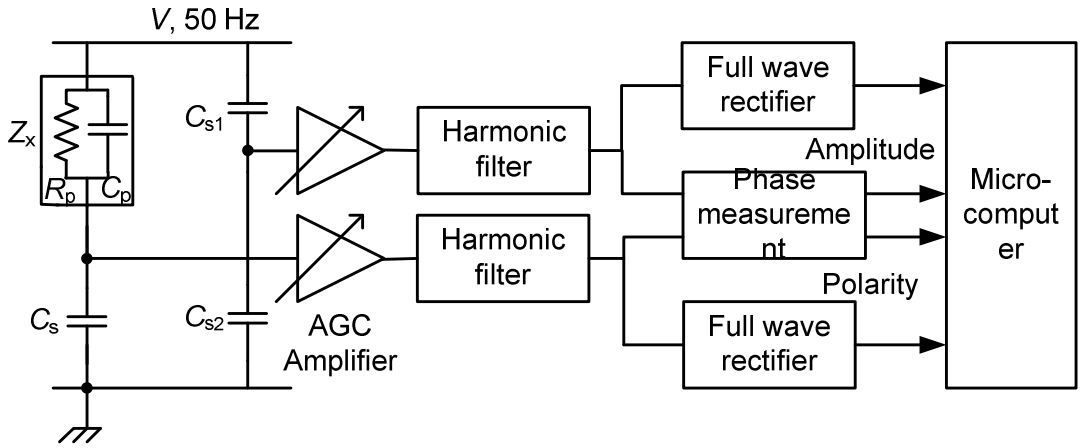

Fig. 2.4 Schematic for measuring dissipation factor based on zero-crossing detection using AGC amplifier [10]

During power-on of instrument the controlling microcomputer calibrates itself by testing the two channels by applying a test waveform to the input channels. All the gain ranges are exercised and their gains are measured as well as stored. Identical signals are applied to both the channels and minor phase offset between them are stored. The output voltage of low pass filter is measured, corrected and displayed according to the calibration result obtained during power-on self-test. The method also incorporates capacitance measurement. Here, the output voltage from two channels is rectified, smoothed, measured and adjusted to take into account the known gain of the AGC amplifiers, obtained during the calibration. The ratio of these two outputs is taken. These outputs correspond to the specimen current and reference input current. The ratio calculated is displayed, giving the capacitance ratio. The instrument was designed for the loss angle in the range of $100\text{-}1000\times10^{-5}$ with an accuracy of $\pm$2% of reading $\pm$ 1×10^{-5}.

2.3 Online monitoring using a bridge method

The main application of this technique in diagnosing the state of current-transformer insulation in a substation is discussed in [4]. Fig.2.5 gives the basic arrangement of this technique. Here the reference voltage is taken from standard gas capacitor (called absolute dissipation factor measurement) or taken from another unit in service (called relative dissipation factor measurement). The two signals U_R and U_M are monitored at a time and processed to get dissipation factor. The computation method of dissipation factor is not specified. The reported method was used to measure the dissipation factor of the current transformer under no load condition with a 275 kV voltage. This technique only recognizes trends and patterns, such as cyclic characteristics, in the results. The reported result shows the variation in the dissipation factor being measured from 500-600×10^{-5} over a period of 12 hours for both absolute and relative dissipation factor measurements. However, the reported method does not give any information about the range, accuracy and resolution of measurement.

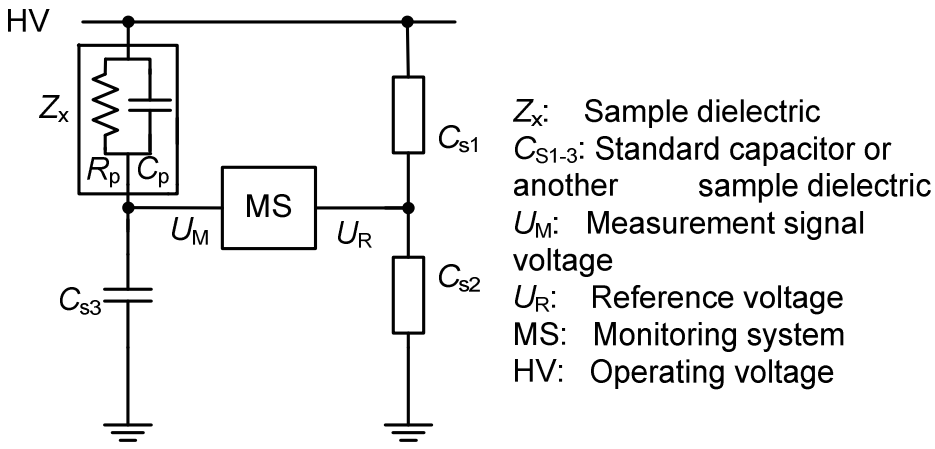

Fig 2.5 Bridge balancing based dissipation factor measurement [4]

2.4 Techniques based on harmonic analysis

One such technique is reported in [5], wherein harmonic analysis using DFT is performed on the acquired current and voltage signals. The measurements are performed on a 230 kV current transformer unit. The analog voltage and current signals are scaled down and passed through signal conditioning unit, which provides low pass filtering and

isolation of input analog signals. An 8-bit resolution digital storage oscilloscope was used to implement the simultaneous sampling of the analog voltage and current signals. The dissipation factor was obtained from the phase information of fundamental components by using DFT. The authors have also reported the effect of sampling rate, effect of line frequency fluctuation and effect of line harmonics. First a laboratory setup was made to measure the dissipation factor of low loss polystyrene capacitor and a metal film resistor under low voltage condition. Subsequently the technique was used to measure the dissipation factor of 500 pF / 40 kV capacitor under high voltage. The precision of measurement reported is $\pm 5\times10^{-5}$ for dielectric dissipation factor ranging from 100-2000×10^{-5}, for signal sampling rate of 200 k Sa/s.

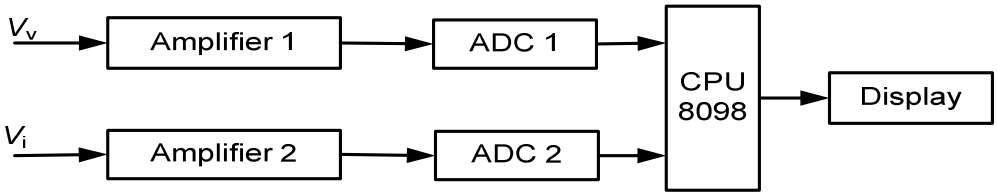

Fig. 2.6 Schematic for measuring dissipation factor and capacitance using FFT [8]

Another technique based on phase measurement using signal processing is reported in [7][8]. It is used for online dissipation factor monitoring of capacitive-type insulation. The schematic arrangement of this measurement technique is shown in Fig. 2.6. The two signals corresponding to bushing current V_i and applied voltage V_v are obtained from current and voltage sensors respectively. Two separate amplifiers amplify these signals and limit the amplitudes, suitable to ADC. The two amplifiers are chosen to have low settling time in order to decrease the phase drift caused by amplifiers. A 12-bit ADC is used to sample the voltage and current signals simultaneously. Let $V_v(t)$ and $V_i(t)$ represents the voltage and current signal respectively, where

$$V_v(t) = U_{v1}\sin(\omega t + \varphi_v) + \sum_{n=2}^{\infty} U_{vn}\sin(\omega n t + \varphi_{vn}) \tag{2.7}$$

$$V_i(t) = U_{i1}\sin(\omega t + \varphi_i) + \sum_{n=2}^{\infty} U_{in}\sin(\omega n t + \varphi_{in}) \tag{2.8}$$

The sampled voltage and current signals are processed using fast Fourier transform (FFT) to obtained fundamental voltage and current signals i.e. $U_{v1}e^{j\varphi_v}$ and $U_{i1}e^{j\varphi_i}$.

$$\frac{U_{v1}e^{j\varphi_v}}{U_{i1}e^{j\varphi_i}} = \left(\frac{U_{v1}}{U_{i1}}\right)e^{j(\varphi_v-\varphi_i)} = \left(\frac{U_{v1}}{U_{i1}}\right)\cos\varphi_{vi} + j\left(\frac{U_{v1}}{U_{i1}}\right)\sin\varphi_{vi} \tag{2.9}$$

We get loss angle as

$$\delta = \varphi_v - \varphi_v = \varphi_{vi} \tag{2.10}$$

which is used to obtain the dissipation factor tan δ. The above technique is implemented using a single chip micro-controller 8098. The micro-controller controls the sampling of signals through ADC's and processes the sampled voltage and current data using FFT to obtain the dissipation factor. Information about the accuracy and range of the instrument developed, using this technique, has not been reported.

2.5 Techniques based on synchronous detection

The technique is reported in [6], and the schematic of measurement setup is shown in Fig. 2.7. It consists of an electro-optic field sensor that is used to sense the voltage on the transmission line. A capacitor, called cap-tap capacitor, is used to sense the insulation current. The cap-tap capacitor is connected in series with the insulation systems. The cap-tap capacitor is chosen to have a very low dissipation factor of its own: $< 50\times10^{-5}$ over the temperature range -40 to 80°C. Capacitance value is chosen to bring down the output voltage into the range of acceptable inputs to electronic systems. The voltage signal measured across cap-tap capacitor, representing the insulation current has a phase difference of δ with the voltage signal obtained from the electro-optic field sensor. Thus the voltage signal from the electro-optic field sensor, representing the applied voltage, is accurately phase shifted by quarter cycle. Then the dissipation factor is computed [29] using

$$\tan\delta = \tan\left[\sin^{-1}\left(\frac{1}{TV_mI_m}\int_0^T v(t)i(t)dt\right)\right] \tag{2.11}$$

where, $v(t) = V_m\sin(\omega t)$ represents the voltage signal obtained from voltage sensor and $i(t) = I_m\cos(\omega t - \delta)$ represents the current signal through the cap-tap capacitor.

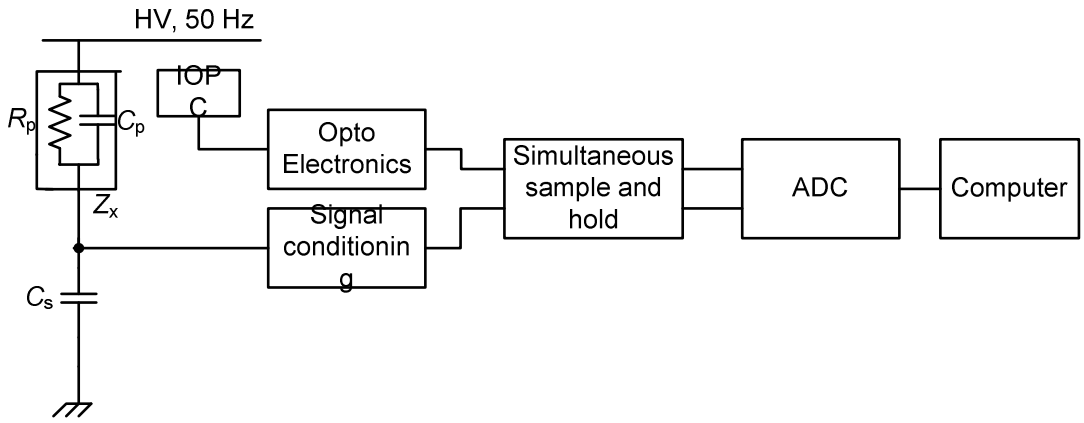

Fig. 2.7 Schematic for measuring dissipation factor using electro-optic sensor [6]

Signal processing unit here consists of ADC paired with a simultaneous sample and hold unit. A computer processes the data and stores the calculated values of the dissipation factor. The two input signals are sampled at a sampling rate of 11.99 kHz. Digitized signals are then low-pass filtered to remove noise and high pass filtered to remove the dc component. The system is designed for power line frequency f_o = 60 Hz. The low-pass filter is a 7^{th} order inverse Chebychev filter with cut-off frequency of 65 Hz, designed to have reached an attenuation of 60 dB by 120 Hz. The high pass filter is a 3^{rd} order inverse Chebychev filter with a cut-off frequency of 55 Hz, designed to have reached an attenuation of 60 dB by 5 Hz. From the filtered signal, the frequency is computed, by counting zero-crossings over a 200-cycle long interval. The number of samples in the quarter cycle is determined using the frequency calculated. Then the voltage signal is shifted by quarter cycle i.e. 90°. Finally dissipation factor is computed as per (2.11). The absolute values of dissipation factors obtained using the set-up is accurate to within $\pm 500\times10^{-5}$ based on the comparisons with the measurements done using conventional bridge technique.

Another measurement method for the phase measurement is reported in [9]. The phase measurement between two distorted periodic signals is based on non-synchronous multi-rate digital filtering. The reported method does not need synchronous sampling as required in the DFT based phase measurement. Therefore it requires only a constant sampling rate. The technique is insensitive to frequency variation in a wide frequency

band around the nominal frequency. For a frequency band of 10% around the nominal frequency, the method can resolve a phase difference of less than 0.5×10^{-5} rad with an uncertainty less than $\pm$ 2.5×10^{-5} rad. The low pass filter based phase measurement is shown in Fig. 2.8.

The two input signals with known sinusoidal and non-sinusoidal test conditions were derived from the programmable power calibrator. It provides a phase resolution of 0.1×10^{-5} rad with an uncertainty of less than 1×10^{-5} rad. The input signals were sampled with an 18 bits ADC with sampling controlled through an external programmable pulse trigger circuit. The two outputs of ADC are passed through digital low pass filters. The outputs of two low pass filters were processed in the processing unit to get the phase shift. For the signals with a phase shift of δ between them, the phase shift is calculated as

$$\delta = cos^{-1}\left(\frac{\sum_{n=k}^{k+K_{2p}-1} v_1h_2(n)v_2h_2(n)}{\sqrt{\sum_{n=k}^{k+K_{2p}-1}(v_1h_2(n))^2 \sum_{n=k}^{k+K_{2p}-1}(v_2h_2(n))^2}} \right) \tag{2.12}$$

where $v_1h_2(n)$ and $v_2h_2(n)$ represent samples at the output of the filters having impulse response as $h_2(n)$ with their respective inputs as v_1 and v_2. The relation gives phase shift around 0 and π. To get phase shift around $\pi/2$, a discrete Hilbert transform [30], as a quadrature phase shifter providing frequency insensitive operation, can be implemented on the output signal from one of the low pass filters $h_2(n)$ and before the input to the processing unit. Then, the phase angle can be obtained from an equation similar to (2.12) using the function $\sin^{-1}(x)$ or $\tan^{-1}(x)$.

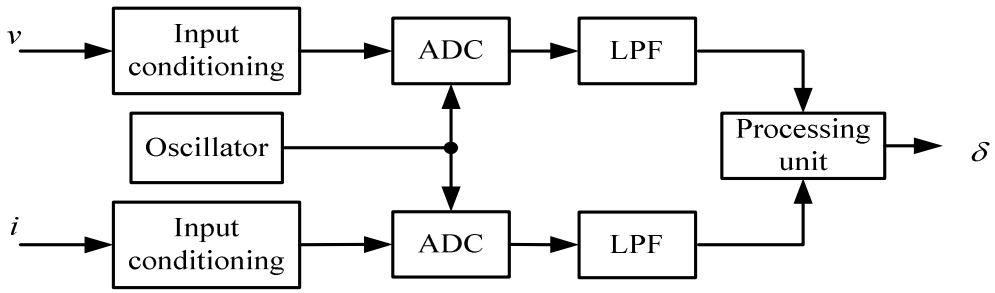

Fig. 2.8 Dissipation factor measurement without multirate filtering (adapted from [9])

If a low pass filter is to be designed for minimum attenuation R_s in the stop band and pass band ripple R_p to be lower than the 1/2 LSB of an L-bit ADC, then the order of the filter becomes very large. For a 16 bits ADC, 1/2 LSB amounts to 0.76×10^{-5}, this corresponds to 6.6×10^{-5} dB for R_p and 102.4 dB for R_s. Low pass filter designed with these specification results in a filter of order 1700. Thus it needs an intensive computation. The filter designed with a pass band ripple of R_p up to the maximum input frequency of f_{max} and stop band attenuation of R_s for input frequency from $2f_{min}$, will have the frequency response shown in Fig. 2.9. Further to avoid the aliasing, the sampling rate has to be higher than the maximum signal frequency components present in the spectrum due to harmonics of fundamental.

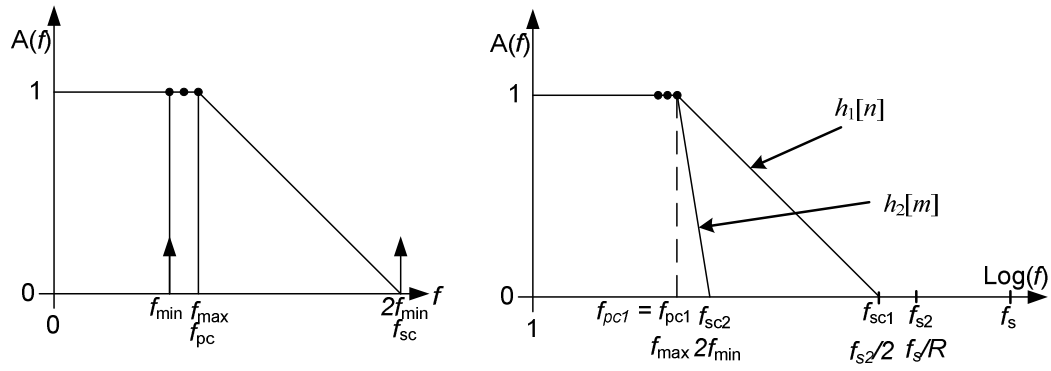

Fig. 2.9 Filtering harmonics with low pass filter and multirate filtering with decimation ratio of R [9]

To overcome aforementioned constraints of single low pass filter, a multi-rate digital filtering is used. Low pass filter $h_2(n)$ used earlier is replaced by the cascade of low pass filter $h_1(n)$, decimation by a factor of R and another low pass filter $h_2(m)$. This approach of processing is shown in Fig. 2.10. The samples of both the preconditioned input signals v_1 and v_2, are sampled at sampling rate f_s (called first sampling rate) are first low pass filtered by $h_1(n)$. This will limit their respective spectra to the low pass filter stop band corner frequency f_{sc1}. The corner frequency of $h_1(n)$ is selected as one half of the second sampling rate f_{s2}. The value of f_{s2} is chosen so as to give an integer ratio of the

first and second sampling rate, *i.e.*, an integer decimation ratio *R*. The decimation ratio is chosen such that another filtering applied with low pass filter $h_2(m)$, at the sampling rate *R* times lower than f_s can filter out fundamental harmonics.

If a low pass filter is designed for a pass band corner frequency f_{pc1} of f_{max} (66 Hz), stop band corner frequency f_{sc1}, with all other R_p, R_s and f_s specification remaining the same, the designed FIR filter will have an order of 97. Similarly the second low pass filter designed for a pass band corner frequency f_{pc2} also of f_{max} (66 Hz), stop band corner frequency f_{sc2} of 2 f_{min} (108 Hz), R_p, R_s as before, the resulting filter will have an order of 210. Thus the two FIR filters designed for an order of 97 and 210, at sampling rates f_s and f_{s2} respectively, are lower than 1700, which is the filter order when only one FIR filter at sampling rate f_s is used. The frequency response of this multirate filter is shown in Fig. 2.9.

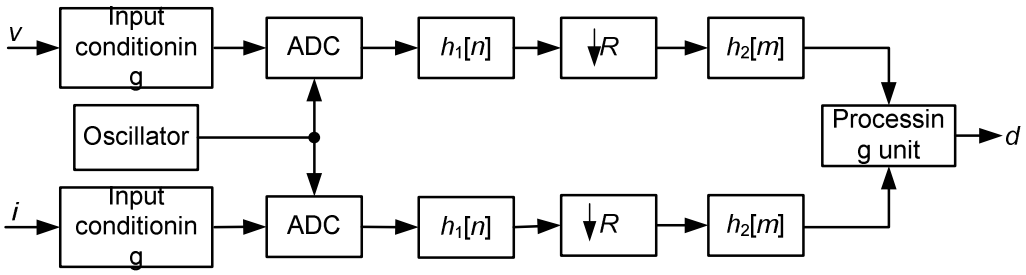

Fig. 2.10 Dissipation factor measurement using multirate digital filtering [9]

The method is tested in the laboratory. The performance of this phase measurement system under different test conditions is reported. These includes a phase measurement of δ and $\pi/2$-δ in the frequency range f_{min} (54 Hz) to f_{max} (66 Hz), and the effect of harmonics in the signal. The results indicates that resolution of phase measurement is less than 0.5×10^{-5} rad and the maximum phase measurement error as a function of measured phase angle in the range of 0 to 2π is less than 2.2×10^{-5} rad. The maximum phase error is less than 2×10^{-5} rad for a harmonic content of 10% in voltage and not more than 50% in current.

2.6 Technique based on decomposition of current signal

Another technique of dielectric loss angle measurement involves the decomposition of reactive and active currents through the dielectric. One such technique is reported in [13]. It is implemented with analog circuit.

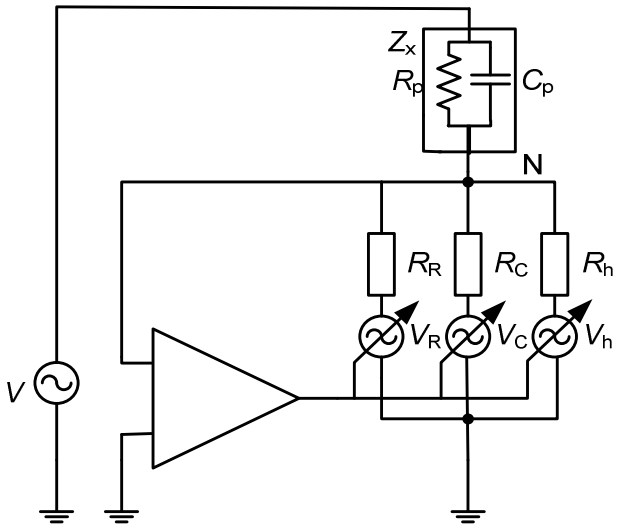

Fig. 2.11 Dissipation factor measurement using adaptive current decomposition [13]

The basic principle of this technique is demonstrated in Fig. 2.11, where V_r, V_c, and V_h represent three adjustable voltage sources. The three voltage sources are adjusted to get zero potential at node N. The three adjustable voltage sources are adjusted to decompose the dielectric current of Z_x into active current, reactive and harmonic current. When the node voltage N is zero, the tested dielectric loss angle δ is expressed as

$$\tan\delta = \frac{i_R}{i_C} = \frac{R_C}{R_R}.\frac{V_R}{V_C} \tag{2.13}$$

Thus measuring of dielectric loss angle involves measurement of V_R and V_C. The circuit realization of this method is shown in Fig. 2.12, where the electrical potential of detection node N is clamped up to zero. Under the unbalanced condition current i_x will flow through the resistor R_2. $A\cos\omega t$ and $A\sin\omega t$ are multiplied with voltage across R_2 in multiplier to get output V_c and V_r respectively. These outputs are low pass filtered using integrators. The output V_c will have $\cos\delta$ and $\cos 2\omega t$, where the frequency component at

second harmonic is removed by integrator (low pass filter) to get only cos δ. Similarly from the output of second integrator we will get sin δ. These cos δ and sin δ are multiplied with the $A\sin\omega t$ and $A\cos\omega t$ to get active and reactive current respectively to make the voltage at node N zero. With voltage at node N zero, the ratio of outputs of two low pass filter gives the dissipation factor tan δ. The accuracy of the instrument based on this method is up to 1% $\pm$ 0.3×10^{-5}.

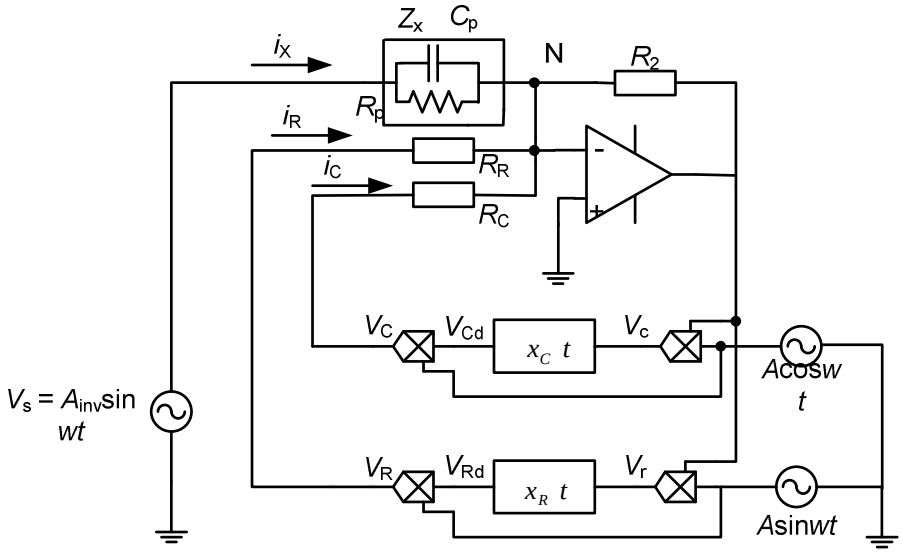

Fig. 2.12 Circuit realization of dissipation factor measurement using adaptive current decomposition [13]

Another technique under this category is reported [16] to measure capacitance and dissipation factor of a capacitor at low voltage. Fig 2.13 shows the block diagram of this measurement technique. This technique incorporates computation of real and imaginary parts of admittance under sinusoidal excitation from voltage across the capacitor and the current through it. The technique of separation of real and imaginary parts of the admittance is realized with a standard capacitor, three-phase sensitive detectors, a constant 90° phase shifter and two digital voltmeters. The ratio of two currents i.e. current in phase with the applied voltage and component in quadrature is taken to compute dissipation factor. First the current through the unknown capacitor Z_x is converted into a voltage signal by op-amp OA1 as shown in the Fig 2.13. Similarly current through standard capacitor C_s is also converted to voltage by another op-amp

OA2. The output of PSD1 and PSD2 consists of a dc component, wherein output V_1 is proportional to the 1/ R_P and V_2 is proportional to the ωC_P.

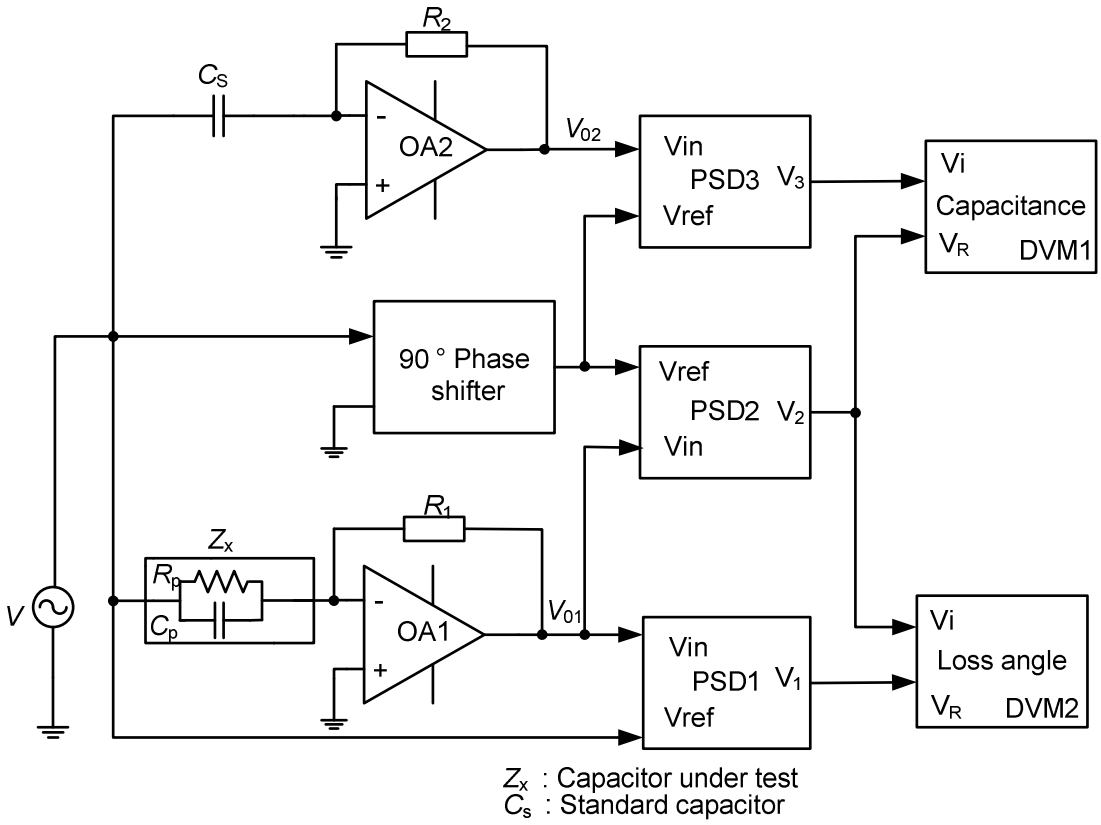

Fig. 2.13 Schematic for measuring dissipation factor and capacitance of capacitor [16]

Finally the ratio of V_1 and V_2 is taken that gives the dissipation factor. The error in the measurement is due to PSDs, because of the non-idealities of the PSD operation, not having exact phase shift of 90°. The reported accuracy of measurement for dissipation factor is $\pm$ 2.5% and that for capacitance is $\pm$ 0.2%.

2.7 Technique based on sum current method

Another approach to determine online dissipation factor is reported in [11][12]. This approach of dissipation factor measurement is illustrated in Fig. 2.14. It is based on the fact that in a three-phase system, if the system voltages are perfectly balanced then vector sum of current vectors is zero, else there will be an imbalance in the current. In this technique, three bushings are excited with three-phase supply. The current through

these bushings are measured as the voltage across a standard capacitor connected in series with the bushings. The capacitors are chosen to have a very low dissipation factor. The voltage signals thus obtained are vectorially added in the voltage summer circuit.

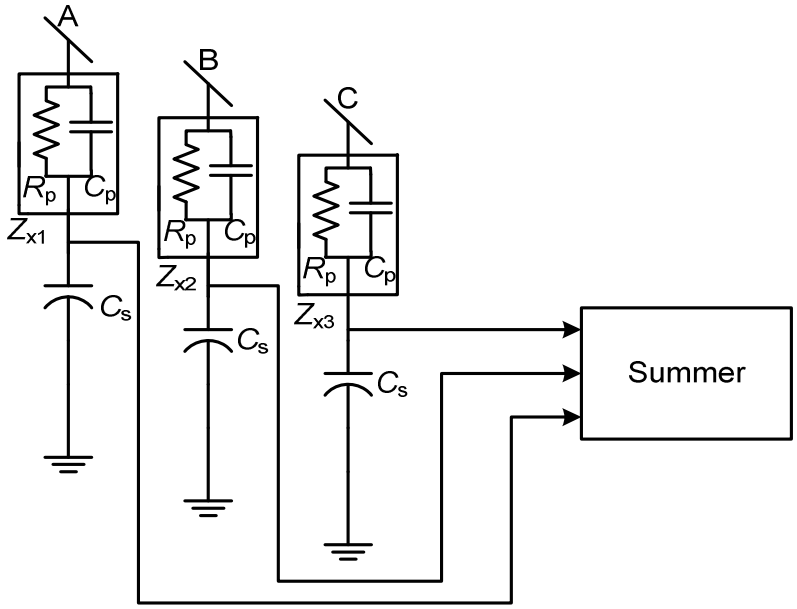

Fig. 2.14 Schematic of measuring dissipation factor using sum current method [11]

If the bushings are identical and system voltages are balanced then the current through all the three bushings will be same. Thus the output of summer will be zero. Practically system voltages are never balanced nor are the bushings identical. When one of the bushings deteriorates, its capacitance and /or power factor will change and hence sum current associated with the set will deviate from its initial value. The vector diagram of current through three-phase bushing set is shown in Fig. 2.15.

During the initial period of installation, system establishes a benchmark sum current I_{Σ}. The voltage across the standard capacitor is current in series with bushing proportional to the sum current and us used as the benchmark output. Later the benchmark is used for comparison with subsequent measurement. Subtracting the benchmark value from the latest measurement of sum current $I_{\Sigma 1}$, gives a third phasor ΔI_{Σ}, which is called 'change in sum current', Fig. 2.15. The angle of this third vector with respect to the reference bushing is used to identify which bushing is causing a change. Once the deteriorated bushing is known, the magnitude and phase of change in the sum

current vector is used to calculate the dissipation factor. But this method has a disadvantage that it calculates the dissipation factor of the bushing experiencing greatest degree of degradation. The method reported does not give any information about the accuracy, range and resolution of measurement.

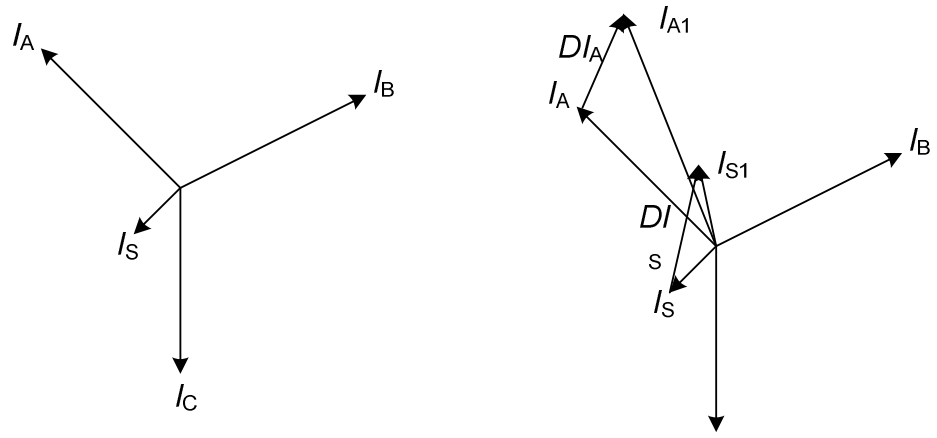

Fig. 2.15 Vector diagram with initial sum current non-zero and change in sum current due to change in bushing current [11]

2.8 Technique based on zero-crossing detection

Another instrument for measurement of loss angle is reported in [19]. Fig.2.16 shows the general schematic of this technique. The voltage and current signals are first converted into rectangular waveforms by means of zero crossing detectors and then the time difference between the pulse edges of the square waveforms are obtained using exclusive OR gate. The time difference is measured using counter circuit with high fixed frequency clock pulses derived from the line using a PLL. PLL is used to generate the high frequency pulses from the line frequency in order to cater to the problem of line frequency fluctuations. The high frequency output signal from PLL is ANDed with the output of phase comparator. ANDed output pulses are counted and directly displayed in terms of degrees. Advantage of this technique is it does not require an accurate crystal clock. The main source of error here is, the presence of harmonic distortions in input wave. In the presence of harmonics, these techniques introduce errors or are unusable if

signals have multiple zero crossings. Also the offsets and drifts in these zero crossing detectors can introduce severe errors. This technique measures the dissipation factor in the range of 100-9900×10^{-5} with a resolution of 100×10^{-5}.

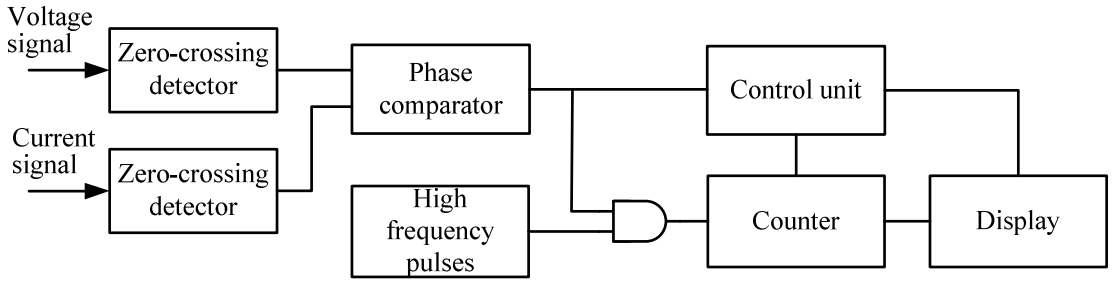

Fig. 2.16 Schematic for measuring dissipation factor using zero-crossing technique [19]

Different methods of phase measurement based on zero crossing are reported in [17][18][20]. However, their application towards the dissipation factor measurement is not reported. These different techniques reported under this category vary in the way the signals are processed, time for computation, and displayed.

2.9 Earlier work done at IIT Bombay

The digital processing technique to measure the dissipation factor is reported in [14][15]. The technique is based on synchronous detection method of phase measurement. Here the dissipation factor is monitored by continuously acquiring the voltage $v(t)$ applied across the capacitor and the current $i(t)$ passing through it and calculating the dissipation factor by dividing the low-pass filtered product of voltage and current signals by the RMS values of the two signals, i.e. by dividing the actual power by apparent power. The processing of signals does not require sampling in synchronism with the power line. Error analysis of this technique was reported for studying the effect of number of quantization bits and other processing parameters.

Solanki [15] carried out a numerical simulation to study the effect of different filters. First LPF used was 10 k tap FIR rectangular window filter with cut-off frequency of 5 Hz with sampling rate of 50 k Sa/s. LPF was redesigned as 4^{th} order IIR Butterworth filter to have monotonically increasing attenuation in the stop band. Next a low voltage

setup was made wherein dissipation factor of a capacitor was measured. Signal acquisition was done using a two channel, 8 bit simultaneous DSO (Tektronix TDS-210). The instrument maximum record length was limited to 2500 samples, thus only 2500 samples could be acquired at a time. The record was transferred using RS-232 interface and "hyper terminal" to a PC. The data acquired were processed to get dissipation factor. Best-fit line relating the dissipation factor measured using the technique versus those obtained from the circuit component has a slope of 1.045 and offset of 66×10^{-5}. Further investigation with high voltage setup was done wherein different dissipation factor were set by using different resistors in series with standard air capacitor. Finally low-cost micro-controller based circuit was made to acquire the signals at sampling rate of 45 Sa/s. The acquired signals were processed in MATLAB. The setup showed errors related to noise in the hardware.

Further investigations are required using good signal acquisition set-up to study the effect of presence of power line harmonics on dissipation factor measurement. Also the effect of quantization needs to be understood in detail. Subsequently filters need to be redesigned with lower cut-off frequency. Finally the dissipation factor measurement needs to be carried at high voltage setups including that of transformer bushing.

Chapter 3

PROPOSED TECHNIQUE AND ERROR ANALYSIS

3.1 Basic technique

The technique involves synchronous detection method of phase measurement. It is based on the principle of sampling the two input signals, proportional to the voltage applied across the capacitor and the current passing through it, and carrying out digital processing of these signals for calculating the dissipation factor, by taking the ratio of actual power to apparent power. The block diagram of the technique is shown in Fig. 3.1.

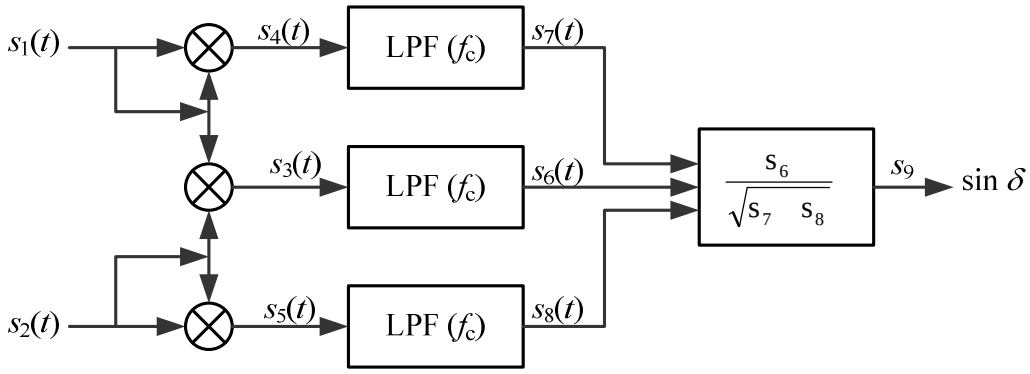

Fig. 3.1 Block diagram of technique used for dissipation factor measurement [14]

The two input signals $s_1(t)$ and $s_2(t)$, are proportional to voltage and current respectively and may be given as

$$s_1(t) = A\ \cos(2\pi f_o t) \tag{3.1}$$

$$s_2(t) = B\ \cos(2\pi f_o t + 0.5\pi - \delta) \tag{3.2}$$

where f_o is the power line frequency and δ is the loss angle. The product of these two waveforms is,

$$s_3(t) = s_1(t)\, s_2(t) = 0.5AB\left[\cos(4\pi f_o t + 0.5\pi - \delta) + \sin\delta\right] \tag{3.3}$$

The squares of the two input waveforms are,

$$s_4(t) = [s_1(t)]^2 = 0.5A^2\ [1 + \cos(4\pi f_o t)] \tag{3.4}$$

$$s_5(t) = [s_2(t)]^2 = 0.5B^2\ [1 + \cos\ 2(2\pi f_o t + 0.5\pi - \delta)] \tag{3.5}$$

These waveforms are low pass filtered with cut off frequency $f_c << f_o$ to retain only the dc components, and we get

$$s_6(t) = \text{LPF}\ \{s_3(t)\} = 0.5AB \sin\delta \tag{3.6}$$

$$s_7(t) = \text{LPF}\ \{s_4(t)\} = 0.5A^2 \tag{3.7}$$

$$s_8(t) = \text{LPF}\ \{s_5(t)\} = 0.5B^2 \tag{3.8}$$

From these equations, we obtain

$$s_9 = s_6 \big/ \sqrt{s_7 s_8} = \sin\delta \tag{3.9}$$

And the dissipation factor is given as,

$$\tan\delta = \tan\left[\sin^{-1} s_9\right] \tag{3.10}$$

Since the value of δ is generally very small, $\cos\delta \approx 1$, hence $\tan\delta \approx \delta \approx \sin\delta = s_9$

3.2 Implementation using digital processing [14]

An analog implementation of this technique will not give accurate and precise measurement because of the errors in the analog multipliers. The scheme can be implemented using digital signal processing after the two signals have been digitized. In this case performance will be limited by quantization noise introduced in the digitization of the waveform and also because of the finite sampling rate. Pandey [14] has carried out a theoretical analysis of the errors.

Error in the estimation of δ will depend on the number of quantization bits L, sampling rate f_s, and filter parameters. The effect of quantization may be modeled as additive random noise [31] [32]. Each quantized and sampled waveform $x(n)$ is the sum of the true signal waveform $s(n)$ and quantization noise $e(n)$. Thus we have,

$$x_1(n) = s_1(n) + e_1(n) \tag{3.11}$$

$$x_2(n) = s_2(n) + e_2(n) \tag{3.12}$$

The signal waveform are given as,

$$s_1(n) = A\ \cos(\omega_o n) \tag{3.13}$$

$$s_2(n) = B\ \cos(\omega_o n + 0.5\pi - \delta) \tag{3.14}$$

where $\omega_o = 2\pi f_o / f_s$ is the digital angular frequency of the power line.

These result in,

$$x_3(n) = x_1(n)x_2(n) = s_1 s_2 + s_1 e_2 + s_2 e_1 + e_1 e_2 \tag{3.15}$$

$$x_4(n) = [x_1(n)]^2 = s_1^2 + e_1^2 + 2s_1 e_1 \tag{3.16}$$

$$x_5(n) = [x_2(n)]^2 = s_2^2 + e_2^2 + 2s_2 e_2 \tag{3.17}$$

After low pass filtering these waveforms, we get

$$\begin{aligned} x_6(n) &= \text{LPF}\{x_3(n)\} = \text{LPF}\{s_1 s_2\} + \text{LPF}\{s_1 e_2 + s_2 e_1 + e_1 e_2\} \\ &= s_6 + e_6 \end{aligned} \tag{3.18}$$

$$\begin{aligned} x_7(n) &= \text{LPF}\{x_4(n)\} = \text{LPF}\{s_1^2\} + \text{LPF}\{e_1^2 + 2s_1 e_1\} \\ &= s_7 + e_7 \end{aligned} \tag{3.19}$$

$$\begin{aligned} x_8(n) &= \text{LPF}\{x_5(n)\} = \text{LPF}\{s_2^2\} + \text{LPF}\{e_2^2 + 2s_2 e_2\} \\ &= s_8 + e_8 \end{aligned} \tag{3.20}$$

where s_6, s_7, s_8 are the true values and the terms e_6, e_7, e_8 have resulted due to quantization noise. We are assuming that the second order harmonic terms have been eliminated by low pass filtering, but a finite amount of broadband quantization noise has remained due to the finite bandwidth of the low pass filter.

Now from x_6, x_7 and x_8 we get,

$$\begin{aligned} x_9 &= \frac{x_6}{\sqrt{(x_7 x_8)}} = \frac{0.5AB\sin\delta + e_6}{\sqrt{(0.5A^2 + e_7)}\sqrt{(0.5B^2 + e_8)}} \\ &= \frac{\sin\delta + 2e_6/AB}{\sqrt{(1 + 2e_7/A^2)}\sqrt{(1 + 2e_8/B^2)}} \end{aligned} \tag{3.21}$$

Assuming the quantization noise magnitudes to be very small compared to the values of *A* and *B*, we get

$$\begin{aligned} x_9 &\approx \left(\sin\delta + \frac{2e_6}{AB}\right)\left(1 - \frac{e_7}{A^2}\right)\left(1 - \frac{e_8}{B^2}\right) \\ &\approx \left(\sin\delta + \frac{2e_6}{AB}\right)\left(1 - \frac{e_7}{A^2} - \frac{e_8}{B^2}\right) \end{aligned}$$

Further, ignoring the second order error terms, we get

$$x_9 \approx \sin\delta + \frac{2e_6}{AB} - \sin\delta\left(\frac{e_7}{A^2} + \frac{e_8}{B^2}\right)$$

$$= \sin\delta + e_9 \tag{3.22}$$

The error term in the final result can be written as,

$$e_9 = (2/AB)e_6 - \sin\delta\left(e_7/A^2 + e_8/B^2\right)$$

$$= 2\,\mathrm{LPF}\{(e_1 s_2 + e_2 s_1 + e_1 e_2)/AB\} - \sin\delta\,\mathrm{LPF}\{(e_1^2 + 2e_1 s_1)/A^2 + (e_2^2 + 2e_2 s_2)/B^2\}$$

Ignoring the second order errors, and combining together the error terms involving e_1 and e_2, we get

$$e_9 = 2\,\mathrm{LPF}\{e_1(s_2/AB - s_1\sin\delta/A^2) + e_2(s_1/AB - s_2\sin\delta/B^2)\}$$

$$= 2\,\mathrm{LPF}\{(e_1/A)(\cos(\omega_o n + \pi/2 - \delta) - \sin\delta\cos(\omega_o n))$$

$$+ (e_2/B)(\cos(\omega_o n) - \sin\delta\cos(\omega_o n + \pi/2 - \delta))\}$$

$$= 2\,\mathrm{LPF}\{(e_1/A)(-\cos\delta\sin(\omega_o n)) + (e_2/B)(\cos\delta\cos(\omega_o n - \delta))\}$$

$$= 2\cos\delta[-(1/A)\mathrm{LPF}\{e_1\sin(\omega_o n)\} + (1/B)\mathrm{LPF}\{e_2\cos(\omega_o n - \delta)\}]$$

We can write the above as,

$$e_9 = 2\cos\delta[-r_1/A + r_2/B] \tag{3.23}$$

where

$$r_1 = \mathrm{LPF}\{e_1\sin(\omega_o n)\} \tag{3.24}$$

$$r_2 = \mathrm{LPF}\{e_2\cos(\omega_o n - \delta)\} \tag{3.25}$$

It is to be noted that r_1 and r_2 are random noises associated with the process of quantization of signals s_1 and s_2 respectively, and hence they are uncorrelated with each other. Therefore, the mean squared value of the error e_9 is given as,

$$\sigma_{e9}^2 = 4\cos^2\delta\left[\sigma_{r1}^2/A^2 + \sigma_{r2}^2/B^2\right] \tag{3.26}$$

For sampling rate of f_s and quantization step of Δ_q, the quantization error [31] [32] can be modeled as random noise with uniform power spectrum density over [$-f_s/2$, $f_s/2$] with ac RMS value given as,

$$\sigma_e = \Delta_q/\sqrt{12} \tag{3.27}$$

In order to estimate the RMS value of the error, we need to obtain estimate of random white noise waveform modulated by a sinusoid and low pass filtered. Let us consider a waveform $p(n)$ generated by multiplying random white noise $e(n)$ having ac RMS value of σ_e with a sinusoidal waveform of frequency f_o ($<f_s/2$),

$$p(n) = e(n)\cos(2\pi f_o n/f_s + \theta) \tag{3.28}$$

Its autocorrelation is,

$$R_p(n) = (1/2)R_e(n)\cos(2\pi f_o n/f_s)$$

and therefore, the power spectrum density (p.s.d.) of $p(n)$ is

$$S_p(f) = (1/4)[S_e(f - f_s) + S_e(f + f_s)]$$

where $S_e(f)$ is the p.s.d. of $e(n)$. Considering $e(n)$ as noise with uniform p.s.d. S_e over $[-f_s/2, f_s/2]$ and RMS value of σ_e, we have

$$S_e = \sigma_e^2/f_s$$

Since $f_s/2 > f_o$, we get the p.s.d. of $p(n)$ as

$$S_p(f) = S_e/2, \text{ for } |f| < f_s/2 - f_o$$

$$S_e/4, \text{ for } f_s/2 - f_o < |f| < f_s/2 + f_o$$

$$0, \text{ for } |f| > f_s/2 + f_o$$

Actually because of aliasing about $f_s/2$, we get

$$S_p(f) = S_e/2, \text{ for } |f| < f_s/2$$

Signal $q(n)$ is the output of the low pass filter $H(f)$. Therefore, the p.s.d. of $q(n)$ is

$$S_q(f) = |H(f)|^2 S_p(f)$$

If the filter has a cut off frequency $f_c < f_s/2 - f_o$, and assuming

$$|H(f)| = 1, \ |f| < f_c$$

$$0, \text{ otherwise}$$

we get,

$$S_q(f) = S_e/2, \text{ for } |f| < f_c$$

$$0, \quad \text{for } |f| > f_c$$

therefore the mean square value of $q(n)$ is given by

$$\sigma_q^2 = (S_e/2)(2f_c) = \sigma_e^2(f_c/f_s)$$

Therefore,

$$\sigma_q = \sigma_e\sqrt{f_c/f_s} \tag{3.29}$$

Using this result, the mean squared value of error e_9 as given in (3.26) may be given as

$$\sigma_{e9}^2 = 4\cos^2\delta(f_c/f_s)(\sigma_{e1}^2/A^2 + \sigma_{e2}^2/B^2) \tag{3.30}$$

For signal range of ($-V_m$, $+V_m$) and L-bit uniform quantization, the quantization step is,

$$\Delta_q = 2V_m/2^L \tag{3.31}$$

and therefore, the ac root mean squared values of the quantization errors in the two inputs are

$$\sigma_{e1} = \sigma_{e2} = \sigma_e = \frac{2V_m}{2^L\sqrt{12}} \tag{3.32}$$

Let the peak value of the two input signals be,

$$A = \alpha_1 V_m$$

$$B = \alpha_2 V_m$$

Then, $$\sigma_{e9} = (2\cos\delta)\left(\frac{1}{2^L}\right)\left(\frac{1}{\sqrt{3}}\right)\sqrt{\left(\frac{1}{\alpha_1^2}+\frac{1}{\alpha_2^2}\right)}\sqrt{\frac{f_c}{f_s}} \tag{3.33}$$

For the special case of $\alpha_1 = \alpha_2 = 1$ (i.e., both the input signals occupy the full range of the ADC's), we get

$$\sigma_{e9} = \sqrt{\frac{8}{3}}\cos\delta\left(\frac{1}{2^L}\right)\sqrt{\frac{f_c}{f_s}}$$

For small values of δ, $\cos\delta \approx 1$ and therefore

$$\sigma_{e9} = \left(\frac{1}{2^L}\right)\sqrt{\frac{8f_c}{3f_s}} \tag{3.34}$$

If we define the normalized cutoff frequency of digital low pass filter as

$$\gamma = f_c / f_s \tag{3.35}$$

then the ac RMS value of the error can be written as

$$\sigma_{e9} = 2^{-L}\sqrt{8\gamma/3} \tag{3.36}$$

The values of σ_{e9} as given by (3.36) are calculated and given in Table 3.1 for some specific values of L and $\gamma = f_c / f_s$. Table 3.2 gives the value of γ for some specific values

of L and σ_{e9}. For condition monitoring of insulation in transformers, dissipation factor of interest is generally in the range 500–5000×10^{-5}. For 1% resolution at the low end of the range, we should have $\sigma_e < 5\times10^{-5}$. To achieve this with L = 8 and 12, we require $\gamma = 6.14\times10^{-5}$ and 15700×10^{-5} respectively. For f_o = 50 Hz and f_s = 900 Sa/s, this will require f_c = 0.055 Hz and 14 Hz respectively.

Table 3.1 Theoretical estimates of RMS values of error, σ_{e9}, caused by input quantization. Number of quantization bits = L, normalized cut-off frequency $\gamma = f_c / f_s$.

L	σ_{e9}					
	γ = **0.5**	γ = **0.1**	γ = **0.01**	γ =10^{-3}	γ = 10^{-4}	γ = 10^{-5}
1	0.58	0.26	0.82e-01	0.26e-01	0.82e-02	0.26e-02
4	0.72e-01	0.32e-01	0.1e-01	0.32e-02	0.1e-02	0.32e-03
8	0.45e-02	0.20e-02	0.64e-03	0.2e-03	0.64e-04	0.2e-04
12	0.28e-03	0.13e-03	0.40e-04	0.13e-04	0.40e-05	0.13e-05
16	0.18e-04	0.79e-05	0.25e-05	0.79e-06	0.25e-06	0.79e-07

Table 3.2 Theoretical estimates of the low pass normalized cut-off frequency γ (= f_c / f_s), for specific values of L and RMS values of error σ_{e9}.

L	γ						
	σ_{e9}=10^{-3}	σ_{e9}=5×10^{-4}	σ_{e9}=10^{-4}	σ_{e9}=5×10^{-5}	σ_{e9}=10^{-5}	σ_{e9}=5×10^{-6}	σ_{e9}=10^{-6}
1	1.50e-06	3.75e-07	1.50e-08	3.75e-09	1.50e-10	3.75e-11	1.50e-12
4	9.60e-05	2.40e-05	9.60e-07	2.40e-07	9.60e-09	2.40e-10	9.60e-11
8	2.50e-02	6.14e-03	2.50e-04	6.14e-05	2.50e-06	6.14e-07	2.50e-08
12	0.5	0.5	6.30e-02	1.57e-02	6.29e-04	1.57e-04	6.29e-06
16	0.5	0.5	0.5	0.5	1.61e-01	4.03e-02	1.61e-03

3.3 Effect of harmonics on dissipation factor

The dissipation factor measurement also depends on the harmonic content of line voltage. Let the two input signals be $v(t)$ and $i(t)$, representing the voltage and the current respectively. Then we can represent voltage and current signals, considering the presence of harmonics as,

$$v(t) = \sum_m A_m \cos(2\pi m f_o t + \varphi_m) \tag{3.37}$$

$$i(t) = \sum_m B_m \cos(2\pi m f_o t + \varphi_m + \pi/2 - \delta_m) \tag{3.38}$$

Then,

$$v(t)i(t) = \sum_k \sum_l A_m \cos(2\pi m f_o t + \varphi_k) B_l \cos(2\pi l f_o t + \varphi_l + \pi/2 - \delta_l) \tag{3.39}$$

During low pass filtering with $f_c < f_o$, all the products terms involving $k \neq l$ are eliminated and hence we get,

$$\text{LPF}\{v(t)i(t)\} = \sum_m 0.5 A_m B_m \cos(\pi/2 - \delta_m) \tag{3.40}$$

$$\text{LPF}\{v^2(t)\} = \sum_m 0.5 A_m^2 \tag{3.41}$$

$$\text{LPF}\{i^2(t)\} = \sum_m 0.5 B_m^2 \tag{3.42}$$

And hence we get the output as,

$$s_9 = \frac{\sum_m A_m B_m \sin\delta_m}{\sqrt{\sum_m A_m^2 \sum_m B_m^2}} \tag{3.43}$$

Assuming the C_p and R_p in the dielectric model of Fig 1.1 in Section 1.1 to be frequency independent, we have

$$B_m = \frac{B_1 A_m m}{A_1} \text{ and } \sin\delta_m \approx \tan\delta_m = (1/m)\tan\delta$$

then the output can be written as,

$$s_9 = \sin\delta \frac{\sqrt{\sum_m A_m^2}}{\sqrt{\sum_m m^2 A_m^2}} \tag{3.44}$$

If the entire THD of d is contributed by m^{th} harmonic component, then for the small value of THD ($md << 1$), the error in dissipation factor ΔD, will be bounded by

$$\frac{\Delta D}{D} < \frac{m^2 - 1}{2} d^2 \tag{3.45}$$

For the typical magnitudes of the harmonic components in power line as given in Table 3.3, the value of total harmonic distortion is 4.42% and the error in dissipation factor using (3.44) is 3.82%. By doing band pass filtering on the voltage and current signals, contribution of harmonic components can be eliminated.

Table 3.3 Typical harmonic content in the power line

Harmonic No.	1	3	5	7	9	11	13	15	17	THD
Percentage of 50 Hz	100	1.50	3.00	2.50	≈ 0	1.00	0.75	0.50	0.50	4.42

3.4 Low pass filter

The low pass filter is designed to give good attenuation for second harmonic and other higher frequencies. If we use FIR filter designed to have notches at the multiple of power line frequency then harmonics can be attenuated significantly. But power line frequency varies and can result in a large variation in the attenuation of the second and other higher harmonics. To address this issue, it is decided to use Chebychev type IIR filter. The low pass filter is designed for large attenuation for second harmonic. The designed filter has ripple in the pass band and monotonically increasing attenuation in the stop band [31]. For reducing the error due to product term at $2f_o$, we need to have gain at this frequency of less than 10^{-8}, i.e. an attenuation of 160 dB. The following specifications were chosen for the filter:

- Pass band ripple < 0.02 dB
- Pass band cut-off frequency f_c = 2 Hz for f_s = 900 Sa/s
- Stop band attenuation of > 200 dB to second harmonic.

The filter designed with these specifications has an order of six. The difference equation is given as

$$y(n) = -\sum_{k=1}^{6} a_k y(n-k) + \sum_{k=0}^{6} b_k x(n-k) \tag{3.46}$$

where,

$a_1 = -5.9632$ $\quad$ $b_0 = 0.0079 \times 10^{-11}$

$a_2 = 14.8170$ $\quad$ $b_1 = 0.0474 \times 10^{-11}$

$a_3 = -19.6359$ $\quad$ $b_2 = 0.1201 \times 10^{-11}$

$a_4 = 14.6378$ $\quad$ $b_3 = 0.1560 \times 10^{-11}$

$a_5 = -5.8199$ $\quad$ $b_4 = 0.1213 \times 10^{-11}$

$a_6 = 0.9642$ $\quad$ $b_5 = 0.0468 \times 10^{-11}$

$b_6 = 0.0081 \times 10^{-11}$

This filter's magnitude response for f_s = 900 Hz over the frequency range 0-200 Hz is shown in Fig. 3.2 and magnitude response for the frequency range 0-2 Hz is shown in Fig. 3.3.

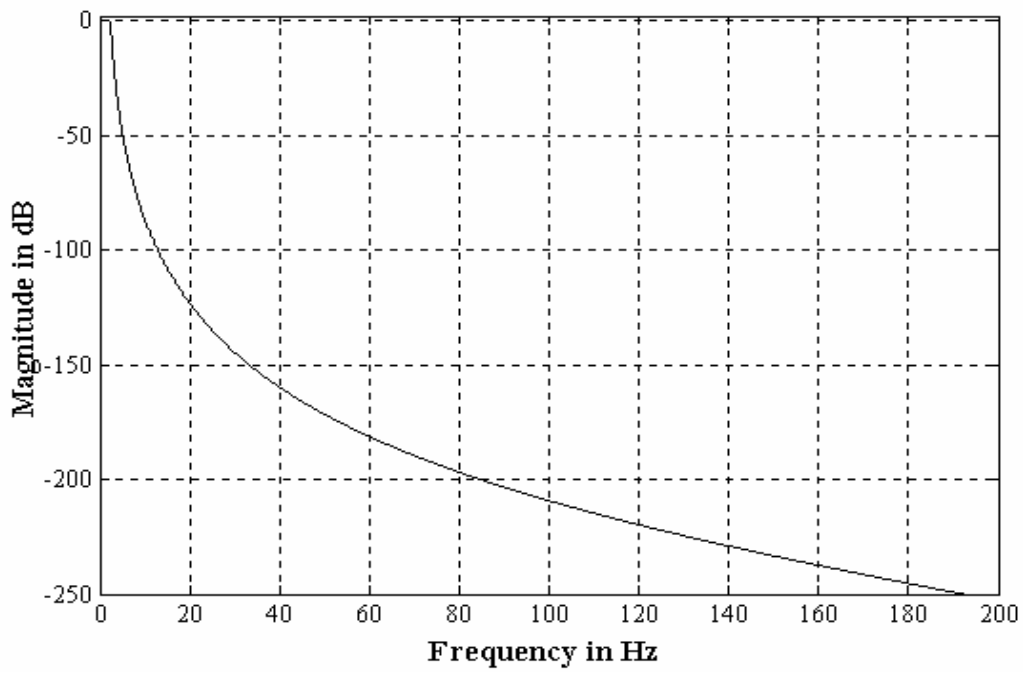

Fig. 3.2 Magnitude response of IIR Chebychev filter with order N = 6, cutoff frequency f_c = 2 Hz, f_s = 900 Sa/s.

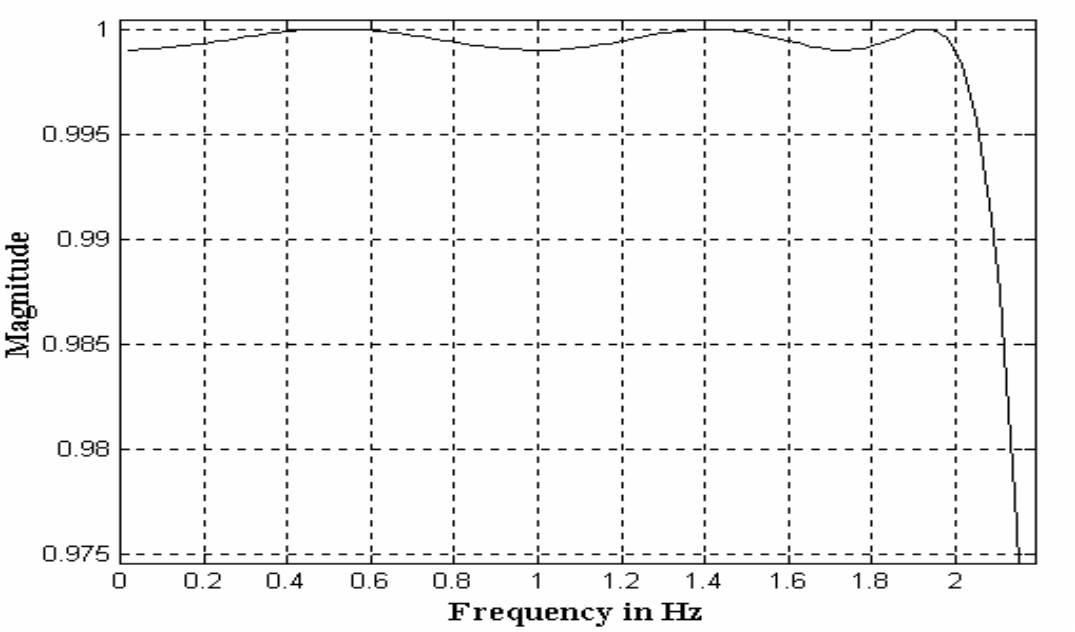

Fig. 3.3 Magnitude response in the pass band 0-2 Hz, of IIR Chebychev filter with order N = 6, cutoff frequency f_c = 2 Hz, f_s = 900 Sa/s.

3.5 Signal processing with low sampling rate

The two waveforms being processed for online measurement of dissipation factor are periodic and when sampled at a low rate will result in aliased periodic sequences, which retain the same phase relationship as the original waveform and thus can be used for obtaining the tan δ values. Let the sampled voltage and current signals from the capacitor with dielectric under test be given as

$$s_1(n) = A\cos(\omega_o n) \tag{3.47}$$

$$s_2(n) = B\cos(\omega_o n + 0.5\pi - \delta) \tag{3.48}$$

where, $\omega_o = 2\pi f_o / f_s$, f_o = power line frequency, sampling rate $f_s > 2f_o$.

Let $f_s < f_o$ with

$$f_x = f_o - f_s \text{ and } \omega_x = 2\pi f_x / f_s \tag{3.49}$$

We get the aliased waveforms as,

$$x_1(n) = A\cos(\omega_x n) \tag{3.50}$$

$$x_2(n) = B\cos(\omega_x + 0.5\pi - \delta) \tag{3.51}$$

We see that the two waveforms x_1 and x_2 are periodic with frequency ω_x, and retain the same phase relationship as s_1 and s_2. The real advantage of the method is that the low sampling rate means a low data rate and processing rate, hence entire hardware can become inexpensive.

Chapter 4
NUMERICAL SIMULATION

Numerical simulation is carried out to serve three different purposes. The first one is the verification of the technique proposed with two different sampling rates (i.e. sampling rate higher than power line frequency and sampling rate lower than the power line frequency). This is done to find out the errors in the measurement contributed by quantization error i.e. the effect of number of ADC bits. Subsequently, to reduce the error due to quantization, band pass filtering of two input signals is carried out and the effect of BPF is studied. The second objective of the simulation is to study the effect of power line frequency variation on the dissipation factor measurement and effect of BPF filtering of input signal in this case. Finally, simulation is done to simulate the condition of presence of harmonics on the power line and its effect on the measurement. The results obtained are presented.

4.1 High sampling rate simulation

To calculate the dissipation factor of the dielectric, we need voltage applied across the capacitor and current through it. Let the voltage and current signal from the dielectric be

$$s_1(n) = A\cos(\omega_o n) \tag{4.1}$$

$$s_2(n) = B\cos(\omega_o n + 0.5\pi - \delta) \tag{4.2}$$

Numerical simulation is carried out with $A = B = 1$, f_o = 50 Hz, and f_s = 900 Sa/s, for loss angle in the range of 100-5000×10^{-5} rad. First, the entire processing is done using a floating-point representation of the waveform in the numerical simulation. Next the effect of L-bit quantization is studied. To simulate the effect of quantization, values in the original waveform in the range -1 to +1 are shifted to a range of 0 to +2 by adding an

offset of 1. The values are then multiplied by 2^{L-1} and rounded to the nearest integer to get integer values over range 0: 2^{L}-1. Next, the values are shifted back to make them bipolar and divided by 2^{L-1} to convert the values back to the original range of -1 to +1. The quantized sequence thus obtained can be written mathematically as

$$s_q(n) = \frac{\text{int}[2^{L-1}(s(n)+1)] - \left(2^{L-1} - 0.5\right)}{2^{L-1}} \tag{4.3}$$

Numerical simulation of the processing is carried out for the voltage and current waveforms synthesized with different values of loss angle δ. The effect of quantization with quantization step Δ_q is basically introduction of a broad band noise, with an overall rms value of $\Delta_q/\sqrt{12}$. Filtering the quantized waveform with a narrow BPF reduces the effect of quantization noise. Processing, both the voltage and current waveforms by the same filter, eliminates phase error introduced by the filter in the final result. It is noted that multiplication of two waveforms of the same frequency and low pass filtering involves synchronous detection, and hence removes the effect of any noise distributed over a wide band. Hence reduction of quantization noise by narrowband filtering of the waveform may not necessarily reduce error in the estimation of loss angle. Thus it is decided to test the merits of using the band pass filter by carrying out the simulation in two modes (a) without BPF and (b) with BPF.

4.1.1 Numerical simulation without BPF

Investigations are carried out for different quantization of the waveform. Simulation is done for floating point, 16-bit, 11-bit, 10-bit, 8-bit, 4-bit, 2-bit, and 1-bit with IIR Chebychev low pass filter, as designed in section 3.4, having cut-off frequency f_c = 2 Hz. The computation is carried out for 9 k length of input samples and the output of filter stabilized after 2.5 k samples. The processed results after stabilization of filter output are used for tabulation. Table 4.1 shows the simulation result for mean s_9 and standard deviation for f_o = 50 Hz, f_s = 900 Sa/s where σ_{s9} shown in the table is the calculated value of standard deviation. Results show that standard deviation obtained from the numerical simulation is less than the calculated σ_{s9} for lower values of δ.

Although the standard deviation obtained is higher for higher values of δ, but by doing different bit quantization it is observed that standard deviation becomes less dependent on quantization as we go for lower bit resolution. It is observed from the result that standard deviation remains nearly same for floating point computation, 16-bit, 11-bit, and 8-bit quantization. However, the errors with respect to set value increase with decreasing L. Also with lower L, the resolution suffers. Simulation with L = 4, 2, 1 showed a very poor performance in the sense that measured output is almost insensitive to input changes. The stabilization of the calculated value of loss angle δ with sample index is shown in Fig 4.1 for loss angle of 50×10^{-5} with 900 Sa/s and L = 16 bit.

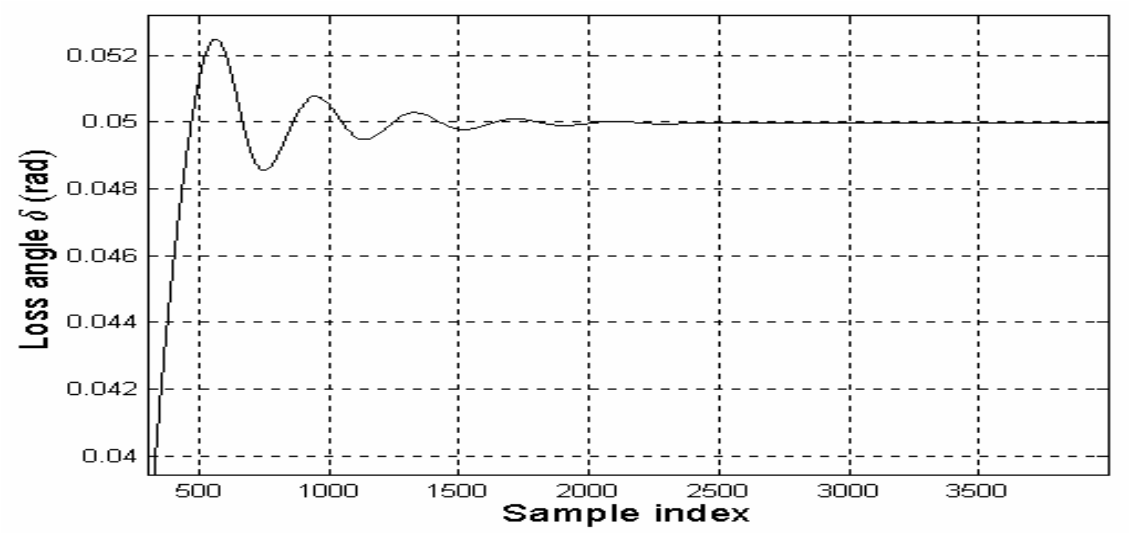

Fig. 4.1 Loss angle δ found from numerical simulation corresponding to 0.05 rad with L = 16 bit and sampling rate of 900 Sa/s

Table 4.1 Results of numerical simulation, without using BPF for γ = 1/450, f_s = 900 Sa/s, and f_c = 2 Hz, for different number of quantization bits.

Set value δ ($\times 10^{-5}$ rad)	**Numerical simulation result, δ ($\times 10^{-5}$ rad)**							
	Floating point		**16-bit integer [$\sigma_{s9} = 0.12\times10^{-5}$]**		**11-bit integer [$\sigma_{s9} = 3.76\times10^{-5}$]**		**8-bit integer [$\sigma_{s9} = 30.07\times10^{-5}$]**	
	Value	**s.d**	**Value**	**s.d**	**Value**	**s.d**	**Value**	**s.d**
100	100	0.02	100	0.02	118	0.03	87	0.02
200	200	0.05	200	0.05	209	0.05	87	0.02
300	300	0.07	300	0.07	304	0.08	253	0.06
400	400	0.10	400	0.10	416	0.10	253	0.06
500	500	0.13	500	0.13	523	0.13	475	0.12
600	600	0.15	599	0.15	610	0.15	774	0.19
700	700	0.18	700	0.18	701	0.18	774	0.19
800	800	0.20	800	0.20	796	0.20	949	0.24
900	900	0.23	900	0.23	904	0.23	949	0.24
1000	1000	0.25	1000	0.25	1015	0.25	978	0.24
2000	2000	0.50	2000	0.50	2017	0.50	2007	0.50
3001	3001	0.75	3002	0.75	3008	0.75	2956	0.74
4002	4003	1.00	4003	1.00	4001	1.00	4187	1.05
5004	5005	1.25	5005	1.25	4988	1.25	5056	1.27

4.1.2 Numerical simulation with BPF

Band pass filtering of the two waveforms are carried out before the calculation of s_9 with the assumption that band pass filter will reduce errors due to quantization error. The band pass filter designed is IIR Chebychev filter having ripple in the pass band and monotonically increasing attenuation in stop band. The band pass filter is designed as a fifth order filter to have pass band as 47-53 Hz. Magnitude response of this band pass filter is shown in Fig 4.2. The computations are carried out for 9 k length of input samples. The output of BPF stabilized after 5 k input samples whereas LPF output

stabilized after 2.5 k samples. Thus the results are computed after 7.5 k input samples. The results of these investigations are tabulated in the Table 4.2. The synthesized sine wave with floating point representation over ± 1 is shown in Fig. 4.3(a). This waveform quantized for data length of 1, 2, and 11 bit along with corresponding output of band pass filter is shown in Fig 4.3. It shows that band pass filter effectively removes the quantization noise. In spite of the reduction in quantization error obtained from band pass filter, it is observed from Table 4.2 that error does not decrease. In fact, there is a small increase in the standard deviation. Thus it may be concluded that BPF does not help in reducing the quantization noise. However, it will still be needed because of the presence of harmonics.

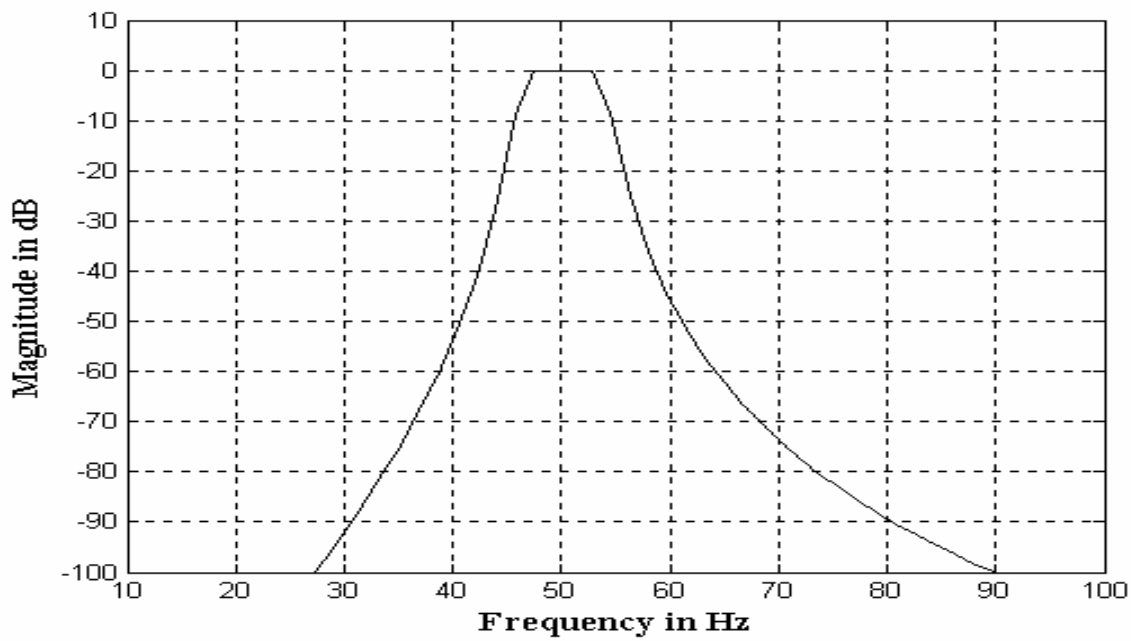

Fig. 4.2 Frequency response of IIR Chebychev BPF with a pass band of 47-53 Hz.

Table 4.2 Results of numerical simulation with BPF for $\gamma = 1/450$ and $f_s = 900$ Hz. LPF: IIR Chebychev filter, $f_c = 2$ Hz, order = 6, 210 dB attenuation at 100 Hz. BPF: IIR Chebychev filter, pass band 47-53 Hz, order = 5, for different number of quantization bits

Set value δ ($\times 10^{-5}$ rad)	**Numerical simulation result, δ ($\times 10^{-5}$ rad)**							
	Floating point		**16-bit integer [$\sigma_{s9} = 0.12\times 10^{-5}$]**		**11-bit integer [$\sigma_{s9} = 3.76\times 10^{-5}$]**		**8-bit integer [$\sigma_{s9} = 30.07\times 10^{-5}$]**	
	Value	**s.d**	**Value**	**s.d**	**Value**	**s.d**	**Value**	**s.d**
100	100	0.07	100	0.07	119	0.08	88	0.06
200	200	0.13	200	0.13	210	0.14	88	0.58
300	300	0.02	300	0.20	304	0.20	253	0.17
400	400	0.27	400	0.27	416	0.28	253	0.17
500	500	0.33	501	0.33	524	0.35	475	0.32
600	600	0.40	599	0.40	611	0.41	774	0.52
700	700	0.47	701	0.47	701	0.47	774	0.52
800	800	0.53	800	0.53	797	0.53	949	0.63
900	901	0.60	900	0.60	904	0.60	949	0.63
1000	1001	0.67	1001	0.67	1016	0.68	978	0.65
2000	2001	1.33	2001	1.33	2017	1.34	2007	1.34
3001	3003	2.00	3004	2.00	3009	2.01	2957	1.97
4002	4005	2.67	4005	2.67	4003	2.67	4188	2.79
5004	5007	3.33	5007	3.34	4990	3.32	5058	3.37

a) Synthesized sine wave with floating point, represented over ±1

b) The waveform of (a) quantized for L = bit

c) The quantized wave -form of (b) after BPF

d) The waveform of (a) quantized for L = 2 bit

e) The quantized wave -form of (d) after BPF

f) The waveform of (a) quantized for L = 11 bit

g) The quantized wave -form of (f) after BPF

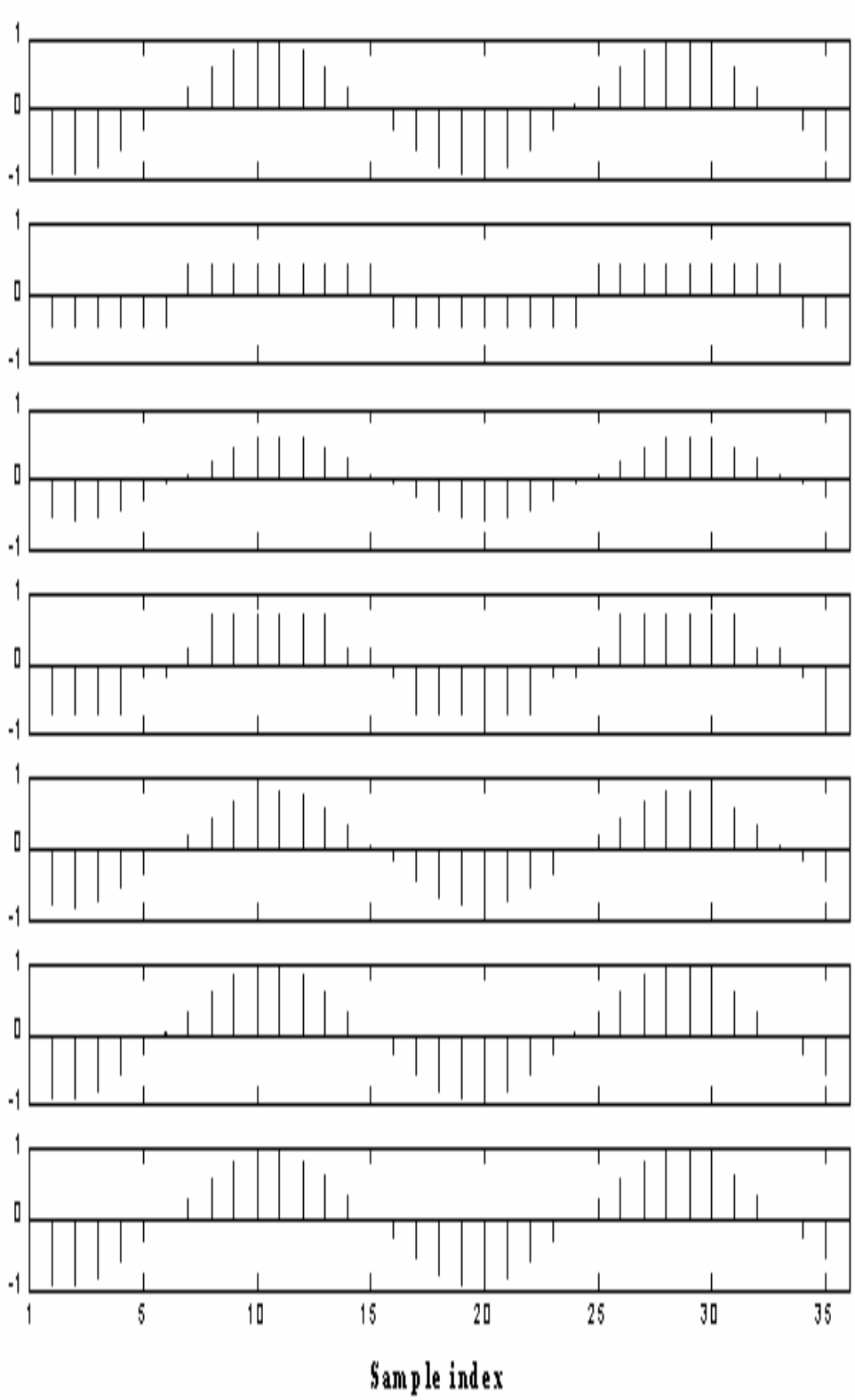

Fig. 4.3 Effect of L bit quantization and BPF on the sinusoidal waveform

4.2 Low sampling rate simulation

For simulation, we have taken $A = B = 1$, signal frequency f_o = 50 Hz, and sampling rate f_s = 45 Sa/s. This results in aliased sinusoidal signals with frequency of 5 Hz. In digital sequence representation, this results in $\omega_0 = 2\pi / 9$ rad/sa. The simulation technique is the same as that in high sampling rate. The numerical simulation are carried using IIR Chebychev low pass filter with a cut-off frequency f_c = 0.1 Hz *i.e.* γ = 1/450. The magnitude response is the same as the one used for high sampling rate but cut-off frequency is shifted to 0.1 Hz. Processing is done for sequence length of 9 k for quantization from 16 bit down to 1-bit.

Table 4.3 Results of numerical simulation without using BPF for γ = 1/450, f_s = 45 Hz

Set value δ ($\times 10^{-5}$ rad)	**Numerical simulation result, δ ($\times 10^{-5}$ rad)**							
	Floating point		**16-bit integer [$\sigma_{s9} = 0.12\times 10^{-5}$]**		**11-bit integer [$\sigma_{s9} = 3.76\times 10^{-5}$]**		**8-bit integer [$\sigma_{s9} = 30.07\times 10^{-5}$]**	
	Value	**s.d**	**Value**	**s.d**	**Value**	**s.d**	**Value**	**s.d**
100	100	0.02	100	0.02	118	0.03	87	0.02
200	200	0.05	200	0.05	209	0.05	87	0.02
300	300	0.07	300	0.07	304	0.08	253	0.06
400	400	0.10	400	0.10	416	0.10	253	0.06
500	500	0.13	501	0.13	523	0.13	475	0.12
600	600	0.15	599	0.15	610	0.15	774	0.19
700	700	0.18	701	0.18	701	0.18	774	0.19
800	800	0.20	800	0.20	796	0.20	949	0.24
900	900	0.23	900	0.23	904	0.23	949	0.24
1000	1000	0.25	1000	0.25	1015	0.26	978	0.25
2000	2000	0.50	2000	0.50	2016	0.51	2007	0.50
3001	3001	0.75	3002	0.75	3008	0.75	2956	0.74
4002	4003	1.00	4003	1.01	4001	1.01	4187	1.05
5004	5005	1.25	5005	3.34	4988	3.32	5056	3.37

The output of filter stabilized after 5 k input samples, and then mean and standard deviation are computed. These results are tabulated in the Table 4.3. On comparing these results with high sampling rate results tabulated in Table 4.1, it is observed that standard deviation obtained for both the sampling rates are nearly equal. Also the errors and resolution are similar.

Like high sampling rate, simulation of processing included band pass filtering of input signals, with a 5^{th} order IIR Chebychev BPF with pass band from 4.7-5.3 Hz. The output of BPF shows a significant reduction in quantization noise but this does not give improvement in the standard deviation, as observed from Table 4.4, as in case of high sampling rate.

Table 4.4 Results of numerical simulation with BPF for $\gamma = 1/450$ and $f_s = 45$ Hz.

Set value δ ($\times 10^{-5}$ rad)	**Numerical simulation result, δ ($\times 10^{-5}$ rad)**							
	Floating point		**16-bit integer [$\sigma_{s9} = 0.12\times10^{-5}$]**		**11-bit integer [$\sigma_{s9} = 3.76\times10^{-5}$]**		**8-bit integer [$\sigma_{s9} = 30.07\times10^{-5}$]**	
	Value	**s.d**	**Value**	**s.d**	**Value**	**s.d**	**Value**	**s.d**
100	100	0.07	101	0.07	119	0.08	88	0.06
200	200	0.13	200	0.13	209	0.14	88	0.06
300	300	0.20	300	0.20	304	0.20	253	0.17
400	400	0.27	400	0.27	416	0.28	253	0.17
500	500	0.33	501	0.33	523	0.35	475	0.32
600	600	0.40	599	0.40	611	0.41	774	0.52
700	700	0.47	701	0.47	701	0.47	774	0.52
800	800	0.53	800	0.53	797	0.53	949	0.63
900	900	0.60	900	0.60	904	0.60	949	0.63
1000	1001	0.67	1001	0.67	1016	0.68	978	0.65
2000	2001	1.33	2001	1.33	2017	1.35	2007	1.34
3001	3002	2.00	3003	2.00	3009	2.01	2958	1.97
4002	4004	2.67	4005	2.67	4003	2.67	4190	2.79
5004	5007	3.33	5007	3.33	4990	3.32	5058	3.37

4.3 Numerical simulation of line frequency variation

Numerical simulation is carried out to study the effect of power line frequency variation on dissipation factor measurement with 11 bit signal representation by using IIR Chebychev filter. Here the frequency variation range is chosen to be from 48 Hz to 52 Hz. The mean and standard deviation are computed as earlier after the filter stabilization for sampling rate of 900 Sa/s and 45 Sa/s. These results are tabulated in the Table 4.5 and 4.6 for two sampling rates. The results show that, dissipation factor has a close match to the calculated values and standard deviation is also comparable to the calculated values. Further the results show that for under-sampling with 11 bits, we get standard deviation which is very much less than the calculated deviation. For higher sampling rate the standard deviation is found to be comparable with calculated value. Also it is observed that BPF does not give any significant improvement in the standard deviation for different line frequencies.

Table 4.5 Results of numerical simulation for line frequency variation: f_s = 900 Sa/s, L = 11 bits, calculated s.d. = 3.76×10^{-5}.

Frequency (Hz)	**Set value δ ($\times10^{-5}$ rad)**	**Numerical simulation result, δ ($\times10^{-5}$ rad)**			
		Without BPF		**With BPF**	
		Value	**s.d**	**Value**	**s.d**
48.3	100	103.4	3.4	103.4	3.1
	500	517.7	3.1	517.8	2.8
	1000	1034.9	1.9	1034.9	2.1
50.0	100	118.0	0.03	119.0	0.08
	500	523.0	0.08	524.0	0.35
	1000	1015.0	0.25	1016.0	0.68
51.7	100	97.2	4.3	97.2	4.1
	500	483.4	5.0	483.4	4.7
	1000	966.4	3.4	966.4	3.2

Table 4.6 Results of numerical simulation for line frequency variation: f_s = 45 Sa/s, L = 11 bits, calculated s.d. = 3.76×10^{-5}

Frequency (Hz)	**Set value δ(×10^{-5} rad)**	**Numerical simulation result, δ(×10^{-5} rad)**			
		Without BPF		**With BPF**	
		Value	**s.d**	**Value**	**s.d**
48.3	100	101.0	0.016	101.6	0.016
	500	510.6	0.08	508.4	0.08
	1000	1032.4	0.16	1030.9	0.16
50.0	100	118.0	0.03	119.0	0.08
	500	523.0	0.13	523.0	0.35
	1000	1015.0	0.2	1016.0	0.68
51.7	100	95.9	0.05	95.7	0.05
	500	487.3	0.10	487.4	0.1
	1000	969.5	0.16	969.4	0.18

Table 4.7 Numerical simulation results for power line harmonics: f_o = 50 Hz, L = 11 bits

Frequency (Sa/s)	**Set value δ(×10^{-5} rad)**	**Numerical simulation result, δ(×10^{-5} rad)**			
		Without BPF [Calculated. s.d. = 3.76×10^{-5}]		**With BPF** [Calculated s.d. = 3.76×10^{-5}]	
		Value	**s.d**	**Value**	**s.d**
900	100	106.7	0.03	105.7	0.07
	500	518.4	0.13	517.7	0.34
	1000	994.6	0.25	995.1	0.66
	5000	4963.6	1.25	4972.9	3.32
45	100	106.7	0.03	105.7	0.07
	500	518.4	0.13	517.8	0.34
	1000	994.6	0.25	995.1	0.66
	5000	4963.6	1.25	4973.0	3.32

4.4 Numerical simulation for power line harmonics

Numerical simulation is done to know the effect of harmonics on dissipation factor measurement. Simulation involved adding harmonic components up to 17^{th} order with THD of 4.42% to power line. The mean and standard deviation are computed as per Eqn 3.44 for set dissipation factor with δ_m, A_m and B_m calculated at different frequency as described in section 3.3. The simulation is carried out for two different sampling rates with and without using BPF. Processing is done after filter output stabilization with both BPF and LPF as done earlier. Results for lower and higher sampling rates are given in Table 4.7. Result show that errors in estimation of loss angle reduce with band pass filtering in both the cases.

4.5 Discussion

Numerical simulation is done to study errors in dissipation factor measurement caused by signal quantization, line frequency variations, and presence of harmonics in input supply voltage. Numerical simulation shows excellent match in the results obtained compared to the values obtained by theoretical analysis. Also, it is found that although pre-processing the waveform does not reduce errors due to quantization noise, it is helpful in reducing the errors due to power line harmonics.

Chapter 5
TESTING WITH A LOSS ANGLE SIMULATOR CIRCUIT

As a first step towards experimental validation of the technique, the proposed technique is tested using a loss angle simulator circuit. This is done to understand some of the practical problems of implementation. Signal acquisition is carried out using a multi-function data acquisition unit, and processing is carried on PC. In this chapter, the experimental setup with simulator circuit is described and results obtained are presented.

5.1 Experimental setup

The block diagram of the implementation of the technique is shown in Fig. 5.1. The signal $s_1(t)$ corresponding to the applied voltage is obtained from the signal generator. This voltage signal is phase shifted to obtain the signal $s_2(t)$ corresponding to the current, by using a phase shifter circuit to produce the phase shift corresponding to the required loss angle to be measured. Signal acquisition unit simultaneously samples the two signals. It is a USB based multi-functions data acquisition unit (specification given in Appendix B). The sampling of the two signals is controlled through the graphical user interface software written in Visual Basic. The two signals are sampled at 900 Sa/s with 11 bit precision using signal acquisition unit, utilizing full range of ADC. The acquired data corresponding to voltage and current signals are processed as per the technique [14] described in Chapter 3, with computations carried out using a program in MATLAB.

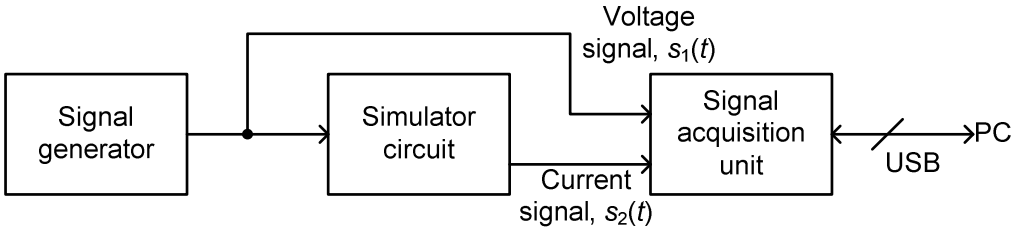

Fig. 5.1. Block diagram of the experimental setup for dissipation factor simulation.

5.2 Loss angle simulator circuit

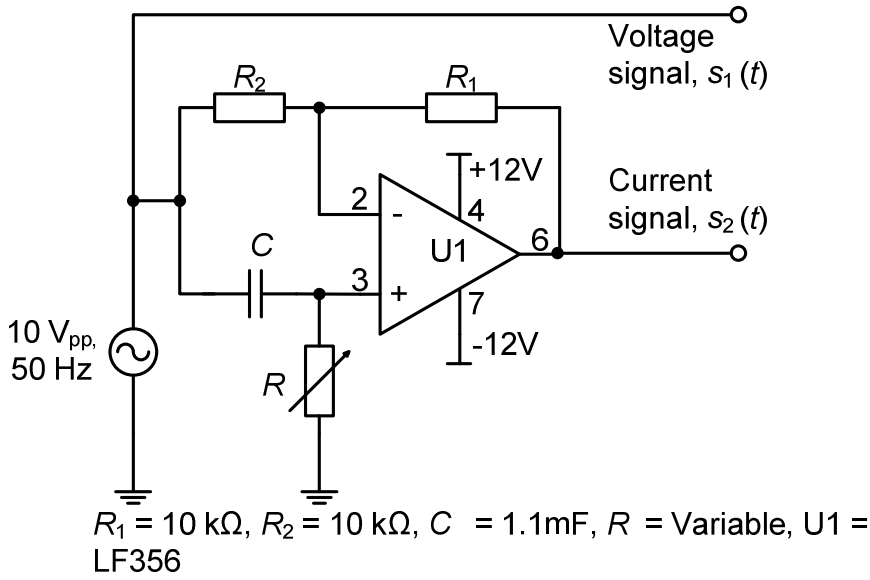

Fig. 5.2. Circuit diagram of phase shifter used as a loss angle simulator.

The loss angle simulator circuit consists of first order all-pass filter to give variable phase shift. The desired phase shift in the signal $s_2(t)$ corresponding to current with respect to the signal $s_1(t)$ corresponding the applied voltage is introduced by changing the value of R in the all-pass filter shown in Fig. 5.2. The circuit acts as first order all-pass filter, with R_1 equal to R_2, the output phase shift is

$$\varphi = \pi - 2\tan^{-1}(2\pi fRC) \tag{5.1}$$

To generate phase shift

$$\varphi = \frac{\pi}{2} - \delta \tag{5.2}$$

between input and output, the value of R can be found from

$$R = \frac{1}{2\pi fC} \tan\{(\frac{\pi}{2} + \delta)/2\} \quad (5.3)$$

With C = 1.1 μF and f = 50 Hz, for $\varphi = \pi/2$, δ = 0, we get R = 2893 Ω. Therefore desired value of δ of either polarity can be achieved by varying R about this value.

5.3 Results

The experiments are carried out for the dissipation factor $D = \tan\delta$ in the range of -100×10^{-5} to 8000×10^{-5}. The variation is simulated by varying the value of R in the simulator circuit at power line frequency of 50 Hz. Signals are digitized with 11 bit resolution, at two sampling rates of 900 Sa/s and 45 Sa/s. These sampled signals are processed as per the algorithm described in section 3.1, using IIR Chebychev low pass filter as described in Section 3.4. The low pass filter used in processing had normalized cut-off frequency of γ = 1/450, *i.e.* f_c = 2 Hz for f_s = 900 Sa/s and f_c = 0.2 Hz for f_s = 45 Sa/s. The outputs are observed after filter stabilization and the mean, standard deviation and error from the set value are tabulated in Table 5.1. The standard deviation in the measured value is found to be less than 14×10^{-5} for f_s = 900 Sa/s and 37×10^{-5} for f_s = 45 Sa/s. For the low pass filter here, with γ= 1/450 and quantization with L = 11 bit, theoretical estimate of the error due to quantization is 4×10^{-5}. The slightly higher error with lower sampling rate may be due to the fact that the attenuation provided by the low pass filter for the harmonic component in the result is lower. For f_s = 900 Sa/s, the second harmonic of 100 Hz occur at a normalized frequency ratio γ= 1/9, where as for 45 Sa/s, the second harmonic occur at γ = 2/9. The measured values of D are plotted against the set values in Fig. 5.3 (I) and Fig. 5.3 (II). We see that the resolution of the measurement is definitely better than the spacing between the set values. In both the cases, there is a good linear relationship between the measured and set values. The best-fit line relating measured value $D_m = (\tan\delta)$ and set value $D_s = (\tan\delta)$, for sampling rate of 900 Sa/s in Fig. 5.3 (I) is given as,

$$D_m = 0.9968\, D_s - 0.0059$$

Similar relation in Fig. 5.3 (II) for sampling rate of 45 Sa/s is,

$$D_m = 0.9953\, D_s - 0.0059$$

In both the cases we see a ratio error of less than 0.5% and offset error ≈ 600×10^{-5}.

Table 5.1 Experimental results obtained from loss angle simulator circuit. The dissipation factor in the first column is calculated for the circuit component values in the phase shifter at frequency of 50 Hz

Set value D_s $(\times 10^{-5})$	**Measured value** D_m, $(\times 10^{-5})$					
	f_s **= 900 Sa/s** $[\sigma_{s9} = 3.76\times10^{-5}]$			f_s **= 45 Sa/s** $[\sigma_{s9} = 3.76\times10^{-5}]$		
	Mean	**Error**	**σ**	**Mean**	**Error**	**σ**
7977	7360	617	7.9	7349	627	19
7062	6453	608	8.2	6463	598	21
6178	5567	609	7.4	5578	599	17
4733	4133	600	7.6	4133	600	18
3752	3147	604	7.0	3151	600	24
2811	2210	600	8.3	2210	600	26
2050	1449	601	13.6	1440	610	24
1750	1154	596	9.5	1145	605	30
1060	465	595	6.3	476	584	22
910	316	594	5.8	327	583	25
886	300	586	7.5	299	587	14
762	169	593	8.2	164	598	4
684	97	587	8.0	85	599	24
623	36	587	10.3	25	598	21
530	-92	622	8.2	-82	612	22
449	-147	596	8.4	-147	596	21
394	-194	588	5.9	-181	575	37
394	-197	591	6.6	-196	590	22
282	-308	590	9.6	-296	578	22
164	-423	587	7.7	-434	598	27
80	-511	591	7.2	-509	589	9
-34	-623	588	8.0	-636	601	25
-106	-692	586	5.1	-699	593	0.35

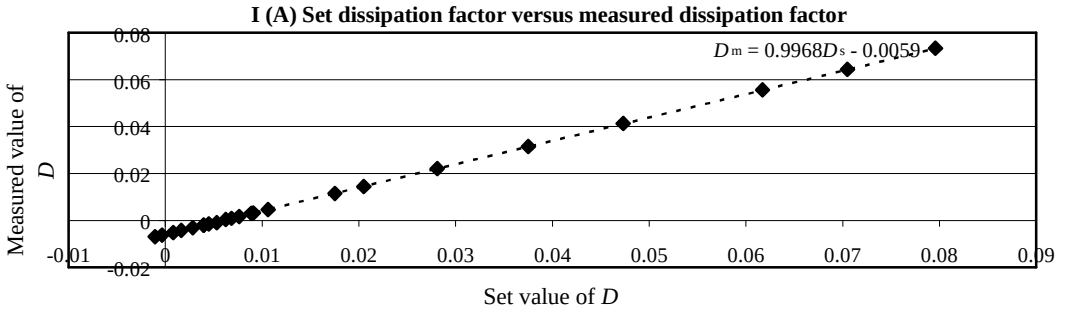

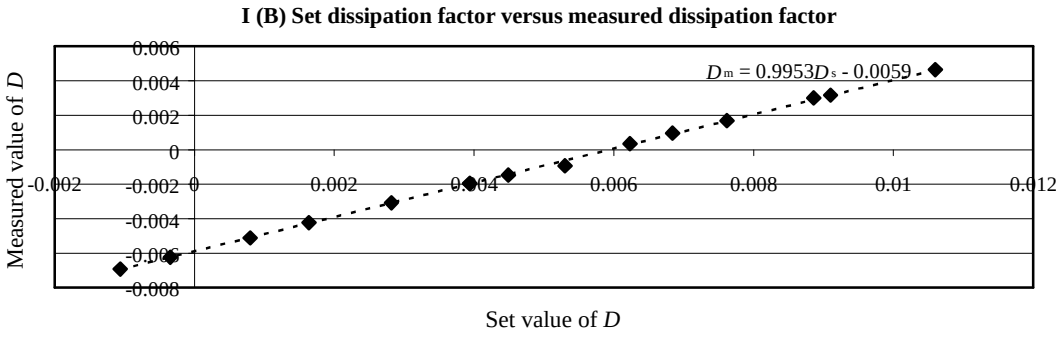

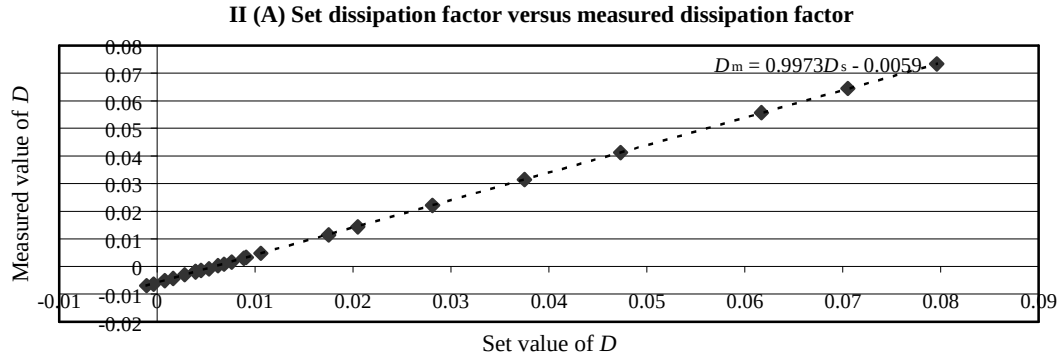

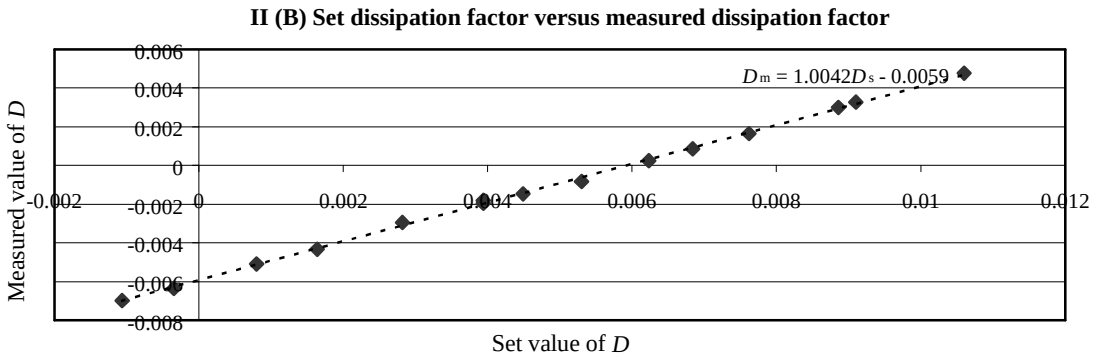

Fig. 5.3 Plot of best-fit line for tan δ for (I) f_s = 900 Sa/s and (II) f_s = 45 Sa/s, with (A) range of -106×10^{-5} to 8000×10^{-5} and (B) range of -200×10^{-5} to 1000×10^{-5}, from the observation given in Table 5.1.

5.4 Discussion

With the experimental setup and loss angle simulator circuit, the proposed technique is tested. The experiments are carried out for the dissipation factor in the range of -100×10^{-5} to 8000×10^{-5} for processing with two sampling rates, with 11-bit quantization of the input waveforms. Results show good linearity between measured and set values. The relationship shows an offset of 600×10^{-5} and ratio error of $< 0.5\%$ Standard deviation in the measurement over the range are less than of 14×10^{-5} and 37×10^{-5} for two sampling rates. In the next chapter, a high voltage setup for measuring dissipation factor of high voltage transformer bushing is presented.

Chapter 6
MEASUREMENT ON DIELECTRIC UNDER HIGH VOLTAGE

In the previous chapter, test results from a loss angle simulator circuit are presented. A high voltage front-end set-up is developed for monitoring dissipation factor of insulation under high voltage use. This front-end circuit provides the signals corresponding to voltage and current, as required by signal acquisition unit. Signal acquisition is done using a PC. Here the dissipation factor of eight bushings rated for 1 kV is measured using the proposed technique. Also, the proposed technique is validated using a standard air capacitor. Results obtained are presented and compared with those from the conventional Schering bridge technique.

6.1 Experimental set-up

Bushings are tested under the field condition for rated voltage of 1 kV, applied from a transformer. The schematic diagram of this experimental set-up is shown in Fig. 6.1. Here an autotransformer T1 is used, which is excited by 50 Hz power line at 230 V. Output of autotransformer is boosted to high voltage by means of a step-up transformer T2 to get 1 kV output.

Scaled down analog signals proportional to the applied voltage and the current through the dielectric are derived by using voltage and current front-end circuits. The voltage front-end consisted of an attenuator and a voltage buffer. The current front-end consisted of a current-to-voltage (I/V) converter. The signal acquisition unit is used to sample the outputs of current and voltage front-end simultaneously.

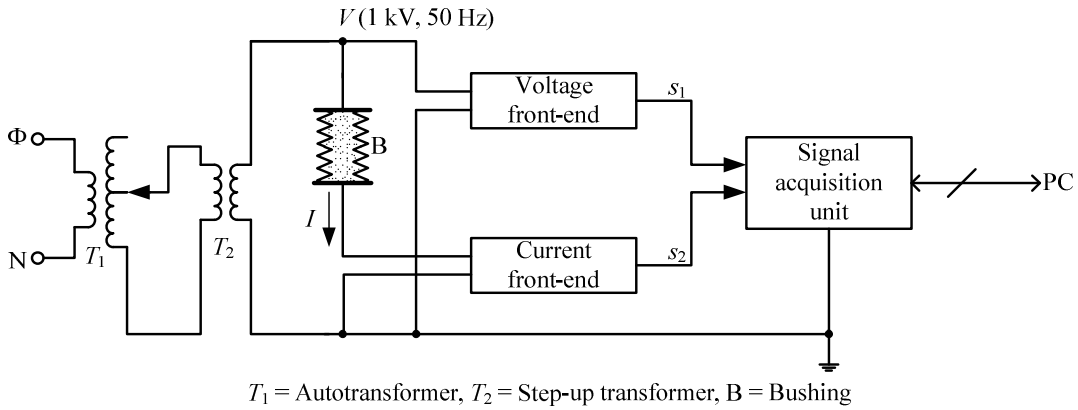

Fig. 6.1 Schematic of experimental set-up. V = Applied voltage, I = Bushing current

The current front-end circuit shown in Fig 6.2 consists of I/V converter for current signal, and the voltage front end shown in Fig. 6.3 consists of an attenuator buffer. Values of components in the circuit are chosen to get peak-to-peak voltage of 5 V at the output of current and voltage front-end circuits. Op-amp U1A is acting as an I/V converter where resistor R_1 is connected in the feedback path of the op-amp for converting the bushing current into a voltage. Resistor R_1 is chosen to get peak-to-peak voltage of 5 V at the output of U1A. Output voltage of U1A is given by

$$V = -IR_1 \tag{6.1}$$

A unity gain inverting amplifier is built using op-amp U1B along with resistors R_3, R_4, and R_5. Op-amp U2A is used as an attenuator buffer along with attenuator resistors R_6 to R_{11} in the voltage front-end circuit. Series combination of resistors R_6 to R_{11} is used to decrease the voltage drop across each resistor on the circuit board. Attenuator resistors are chosen to get, peak-to-peak voltage of 5 V.

In the circuit of Fig. 6.2 and 6.3, diodes D1, D2, D3 and D4 are used to protect the op-amp inputs from high voltage. Op-amps are part of dual op-amp chip CA3240A. It is selected for very low input bias current and very low offset current with very high input impedance. In the set-up, sampling rate and number of samples to be acquired are controlled by graphic user interface program written in Visual Basic. These acquired data are transferred to PC and finally processed using MATLAB to get dissipation factor.

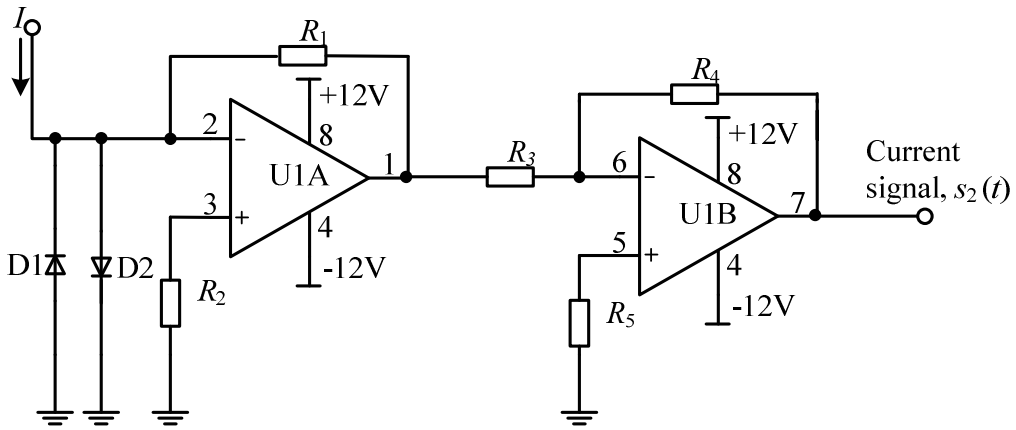

R_1=R_2=22 kΩ, R_3=R_4=6.8 kΩ, R_5=5.1 kΩ, U1=CA3240A, D1=D2=1N4007

Fig. 6.2 Circuit diagram of current front end, I = Bushing current

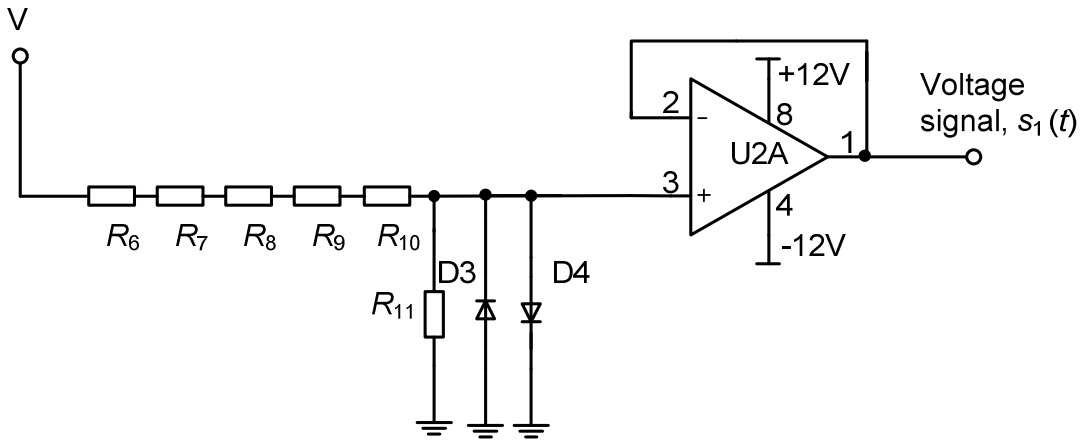

R_6=R_7=R_8=R_9=R_{10}=470 kΩ, R_{11}=3.9 kΩ, U2A=CA3240A,
D3=D4=1N4007

Fig. 6.3 Circuit diagram of voltage front end. V = Applied voltage

6.2 Spectral analysis

The voltage and current signal are acquired using the signal acquisition unit and data are transferred via USB port. The signal acquisition is carried out with sampling rate of 900 Sa/s and records of 21330 samples are stored for signal analysis. The signals are continuously acquired for a period of one hour at an interval of 2-3 minute. For a 1 kV transformer bushing (C = 230 pF, D = 2.3×10^{-5} as measured using Schering bridge) is used as the test object. The frequency spectra of current and voltage signals are computed.

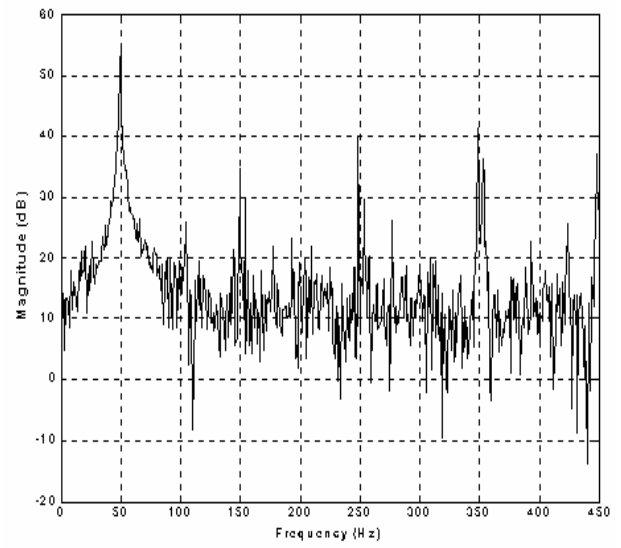

Fig. 6.4 Frequency spectrum of sampled current signal

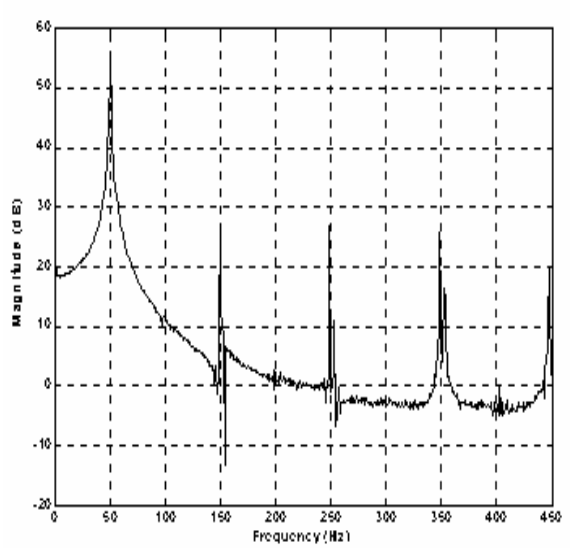

Fig. 6.5 Frequency spectrum of sampled voltage signal

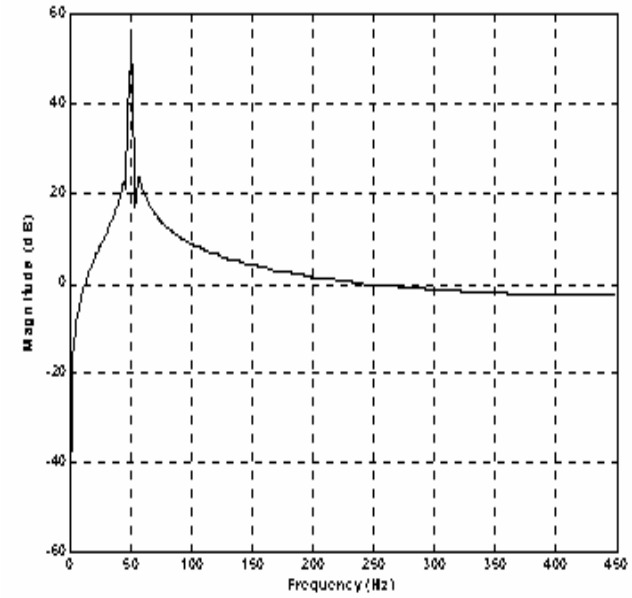

Fig. 6.6 Frequency spectrum of sampled current signal after BPF

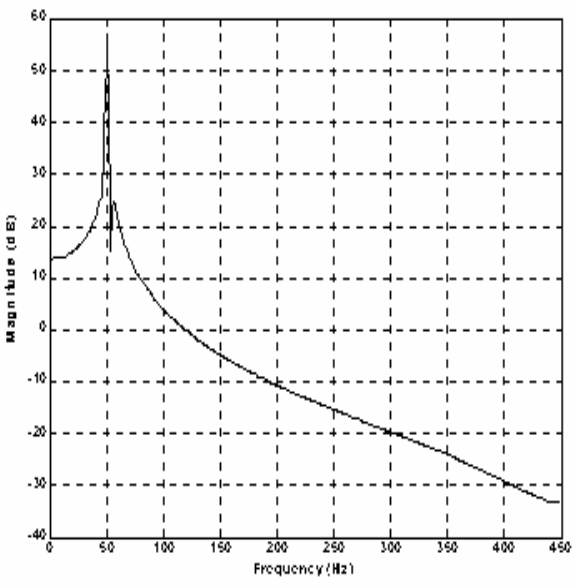

Fig. 6.7 Frequency spectrum of sampled voltage signal after BPF

The frequency spectrum of current and voltage are plotted in Fig. 6.4 and Fig. 6.5 respectively. Frequency spectrum indicates the presence of harmonics of power line frequency and very low frequencies. It also shows a second harmonic which is 17 dB below the main lobe. This may be due to spectral leaking because of the zero-padding used in the FFT computation. However, the total distortion in the signals is computed over a period of one hour to find the variation in the total distortion. It shows a total distortion of about 10% in voltage signal and 35% in current signal. Thus, it is decided to band pass filter the two signals to remove the harmonic components from the signal, before doing any further processing. The two signals are band pass filtered using IIR Chebychev filter of 5^{th} order, with a pass band of 0.104π-0.118π rad/sa. The frequency spectrum of current and voltage signal obtained after BPF is shown in Fig. 6.6 and Fig. 6.7 respectively. It shows reduction in the harmonic components. Total distortion after BPF is also computed and there is a reduction in total distortion in the current as well as in voltage signal. In Fig. 6.8, the total distortions in the two waveforms, without and with band pass filtering are plotted, for readings spread over a 2 hours duration. Total distortion in current is reduced from 35% to 5% while that in voltage is reduced from 10% to 5%.

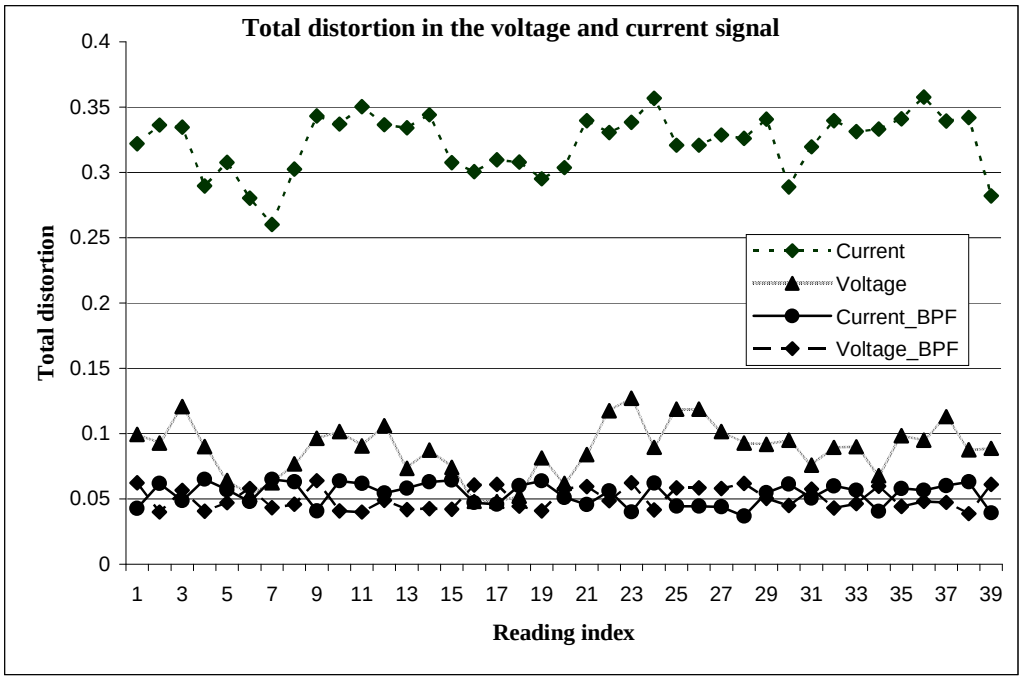

Fig. 6.8 Total distortion in voltage and current signal, before and after BPF

6.3 Experimental results with standard air capacitor

Monitoring of dissipation factor of eight transformer bushings under high voltage is carried out using the experimental set-up. They all showed a drift in the measured dissipation factor with time. The variations could not be linked to variation in power line harmonics or other parameters in the measurement set-up. Hence it is suspected that dissipation factor of bushings may be actually drifting. Subsequently, measurement of the dissipation factor of one of these bushings using a Schering bridge, with bushing left under high voltage for about 2 hours, showed a drift in the dissipation factor with time. Hence to validate the results of online technique, a standard tan δ set is devised. It consist of a standard air capacitor and a series resistance, with tan δ given by

$$\tan \delta = \omega CR$$

We have used C = 1000 pF / 2 kV. With R = 2.869 kΩ, we get tan $\delta \approx 100\times10^{-5}$. Standard tan δ set is first tested for the consistency of its value using Schering bridge. Here the tan δ is measured continuously over a period of 2 hours with applied voltage of 840 V at power line frequency of 50 Hz. The result obtained did not show any variation in tan δ and is observed to be consistently 100×10^{-5}. After the confirmation of the value of the standard tan δ set, different tan δ values are obtained by connecting different resistors in series with the standard tan δ set as given in Table 6.1.

Table 6.1 Different resistor used and dissipation factor value obtained

Resistor value	**tan δ ($\times10^{-5}$)**
12.9 kΩ	489
20.2 kΩ	687
25.5 kΩ	901
94.7 kΩ	3070
159.6 kΩ	5085

Both the voltage and current signals are acquired using the same voltage and current front-end circuit used earlier at sampling rate of 900 Sa/s. The signals are first preprocessed using the BPF to remove the dc and harmonic and then processed using the

online technique. LPF used is IIR Chebychev filter redesigned for lower cut-off frequency of $\omega_C = 0.62\times10^{-3}\pi$ rad/sa. Measurement is carried out by setting different tan δ in the range of 500-5000$\times10^{-5}$ by using different resistor in series with the standard tan δ set.

Table 6.2 Experimental results of online technique using standard air capacitor

tan δ ($\times10^{-5}$)		
Schering bridge	**Online technique**	
	Mean	**s.d. [$\sigma_{s9} = 0.44\times10^{-5}$]**
489	447.1	6.9
687	717.8	5.4
901	922.9	5.1
307	3387.2	4.1
5085	5668.7	3.7

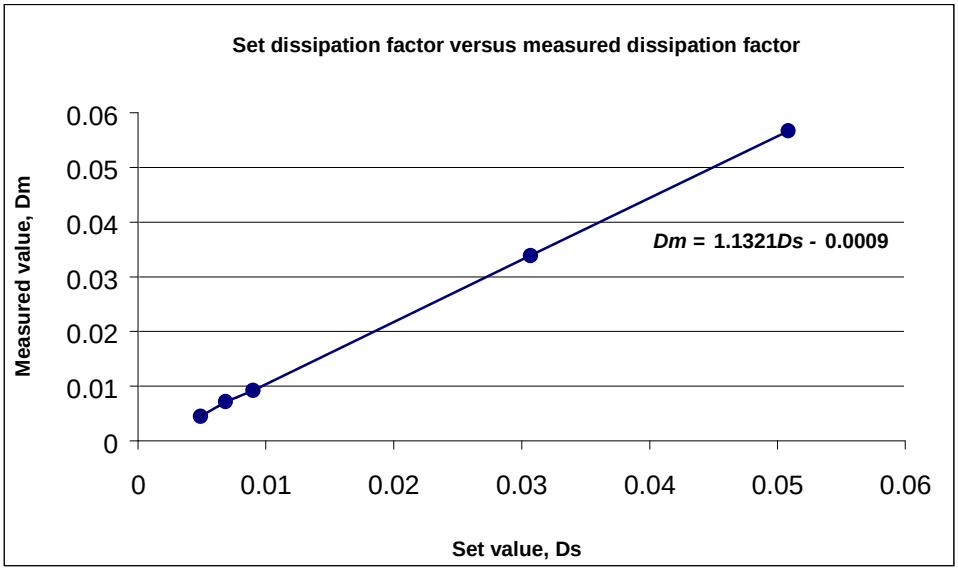

Fig. 6.9 Plot of best-fit line for tan δ in the range of 500-5000$\times10^{-5}$ from the observation given in Table 6.1, for sampling rate of 900 Sa/s. Set values of D_s are found from Schering bridge.

Experimental results of mean and standard deviation obtained are tabulated in Table 6.2. The measured values of D are plotted against the set values in Fig. 6.9. Result shows a very linear relationship between the measured and set values. The best-fit line relating $D_m = (\tan\delta)$ and $D_s = (\tan\delta)$, for sampling rate of 900 Sa/s in Fig. 6.10 is given as,

$$D_m = 1.13\, D_s - 0.0009$$

Thus we get an offset of 90×10^{-5} and ratio error of 13%. The standard deviation in the measured value is $3.7\text{-}6.91\times10^{-5}$ which is comparable to theoretical estimate of the error due to quantization as 0.4×10^{-5}.

Next, to check the effect of different filters on the measured value of dissipation factor, processing is done with IIR and FIR filters. The tan δ is measured continuously over a period of 2 hours and computation done at every 2 minute interval. The results obtained from the IIR Chebychev filter ($\omega_C = 0.62\times10^{-3}\pi$ rad/sa) and those obtained from FIR Hamming window filter (L = 9000, $\omega_C = 14.67\times10^{-5}\pi$ rad/sa) are plotted in Fig. 6.10. Result shows similar performance from both these filters.

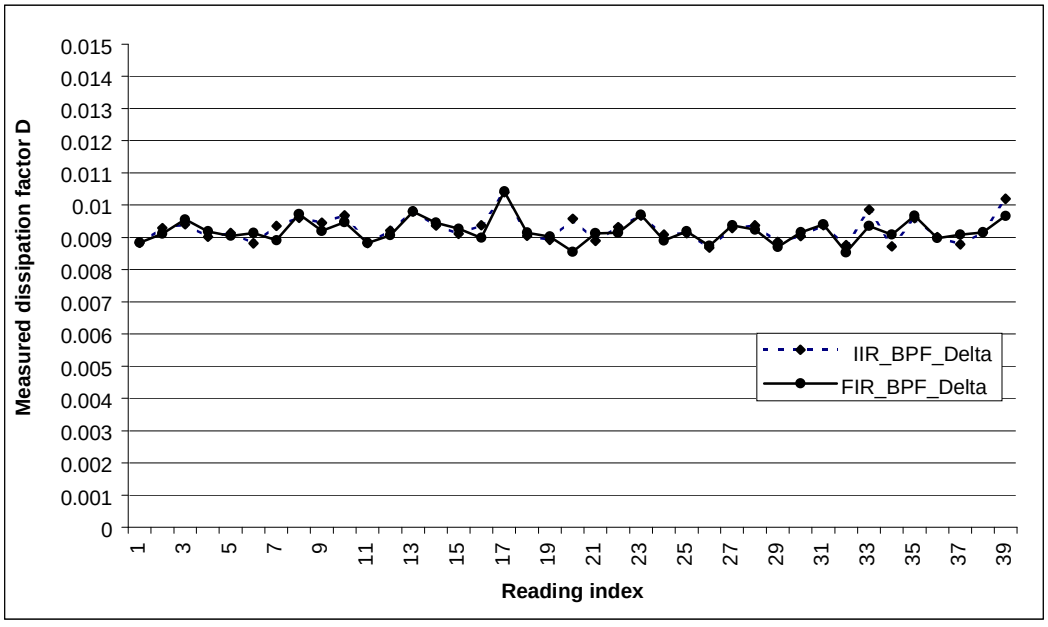

Fig. 6.10 Dissipation factor obtained for standard capacitor using IIR Chebychev filter, and FIR Hamming window filter

6.4 Experimental results with transformer bushing

The dissipation factor of eight bushings is measured using the conventional Schering bridge method. The results obtained are recorded for comparison with those obtained using the proposed technique. These results are given in Table 6.3. Next the experimental set-up described earlier is used to measure the dissipation factor of eight bushings with the proposed technique. The voltage and current signal are acquired as usual with signal acquisition unit and data are transferred via USB port. The signal acquisition is carried out with sampling rate of 900 Sa/s and records of 21330 samples are stored for processing. First preprocessing is carried out with band pass filter and then further processing done to compute the dissipation factor. For low pass filtering in the measurement technique, IIR Chebychev filter with cut-off of $\omega_C = 0.06\times10^{-3}\pi$ rad/sa i.e. $\gamma = 3\times10^{-5}$ is used. Results obtained using online technique is given in Table 6.3.

Table 6.3 Experimental results of dissipation factor of transformer bushings

Bushing No.	**tan δ ($\times10^{-5}$)**				
	Measured using Schering bridge	**Measured using online technique**			
		Measurement 1		**Measurement 2**	
		Mean	**s.d.**	**Mean**	**s.d**
5(1-2)	220	580	560	530	690
5(3-2)	220	480	830	540	620
8(3-2)	240	550	10	530	600
8(1-2)	250	700	820	450	680
13(3-2)	260	500	580	450	650
13(1-2)	260	600	1240	490	720
15(1-2)	6960	6080	1230	6060	640
15(3-2)	7420	6040	1380	6030	780

Result obtained for transformer bushing showed a large variation in the measured value. Also the standard deviation obtained is of the order of 10^{-3} that is also very high.

To check for the variation in the dissipation factor with time, bushings are continuously monitored over a period of 2 hours and dissipation factor is computed at an interval of 2-3 minutes. Acquired data are first preprocessed using BPF as earlier. Then data processing involved three different types of low pass filters. For low pass filtering in the measurement technique, several type of low pass filter are experimented with, (i) IIR Chebychev filter with cut-off frequency $\omega_C = 0.06\times10^{-3}\pi$ rad/sa i.e. $\gamma = 3\times10^{-5}$, (ii) Hamming window based order 9000 FIR filter, with $\omega_C = 14.67\times10^{-5}\ \pi$ rad/sa i.e. $\gamma = 7.3\times10^{-5}$ and (iii) cascading of (i) and (ii) together. The dissipation factor and standard deviation obtained for with these filters are plotted in Fig. 6.11 and Fig. 6.12 respectively. Plot shows similarity in the result, with identical variation in the dissipation factor of the bushing, independent of the filter used. Result show a variation of $400\text{-}800\times10^{-5}$ in the mean value and 150×10^{-5} in the standard deviation.

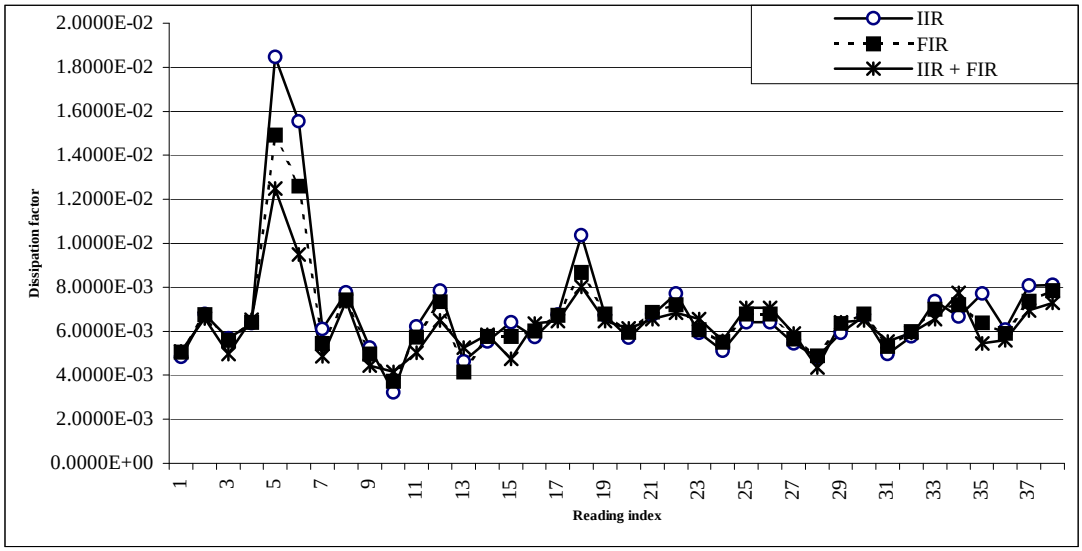

Fig. 6.11 Dissipation factor obtained for transformer bushing using IIR Chebychev filter, FIR Hamming window, and cascade of IIR with FIR filter

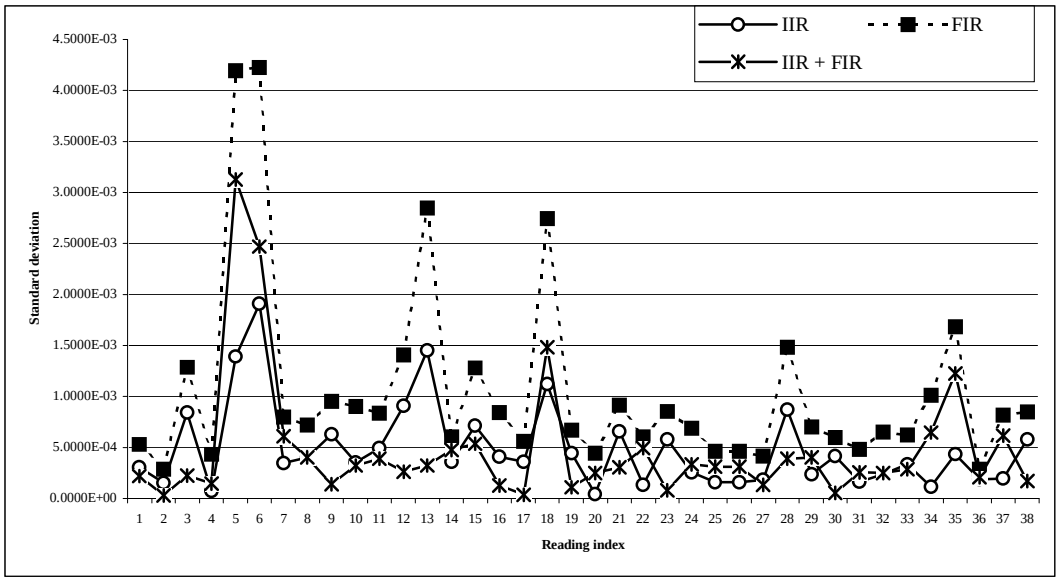

Fig. 6.12 Standard deviation in dissipation factor of transformer bushing using IIR Chebychev filter, FIR Hamming window, and cascade of IIR with FIR filter

To confirm for the variation, bushings are tested on different days continuously over a period of 2 hour using Schering bridge. Test results on different days with Schering bridge on the same bushing shows a variation from 362×10^{-5} to 650×10^{-5}, while on the same day it shows a variation from 362×10^{-5} to 440×10^{-5}. It is to be noted that we cannot carryout Schering bridge and online monitoring simultaneously. Hence, an accurate comparison of online mean with that obtained from Schering bridge could not be carried out for transformer bushing.

6.5 Discussion

A hardware set-up is made to acquire the current and voltage signal from the bushing. A high voltage front end is developed to test the bushing with the rated voltage. Signal conditioning circuit consisting of I/V converter and voltage follower is made to give peak-to-peak voltage of 5 V corresponding to current and voltage signal. These signals are simultaneously sampled through signal acquisition unit at 900 Sa/s and processed on PC using MATLAB to get the dissipation factor. Signal analysis is done to find out the total distortion and frequency spectrum of the signals. The amount of harmonic distortion in the waveforms thus necessitated use of band pass filter of the two

waveforms. Preprocessing brought the harmonic distortion to below 5%. Monitoring of transformer bushing dissipation factor gave large variation, and it is suspected that its dissipation factor might be varying. This is later confirmed, by measurement using Schering bridge. Therefore to validate the technique of online monitoring, a standard air capacitor with different values of series resistor is used. Here, different dissipation factor is set by connecting different resistors in series to realize capacitor with different tan δ. Measurement using online monitoring set-up are carried out for different values of dissipation factor. The results obtained are very close to those obtained using Schering bridge, with an excellent agreement between the two measurements. For measurement with dissipation factor spread over $500–5000\times10^{-5}$, the linear approximation showed an offset of 90×10^{-5} and a ratio error of 13%. The standard deviation of measurements is in the range of $3.7–6.9\times10^{-5}$. These results show that the technique can be used for developing an instrument for online monitoring of tan δ, over the range of $500–5000\times10^{-5}$ with a resolution better than 100×10^{-5}. For better resolution, we will have to increase ADC quantization bits, increase sampling rate, or use filter with sharp cutoff.

Chapter 7

SUMMARY AND CONCLUSIONS

The project involved validation of a technique for online monitoring of high voltage dielectrics, by numerical simulation, and hardware implementation. The objective is to develop instrumentation for online measurement of dissipation factor of transformer bushings in the range of 500-5000×10^{-5}, with a resolution better than 5×10^{-5}. The technique is based on synchronous detection method of phase measurement. The dissipation factor is obtained by processing the simultaneously sampled signals corresponding to voltage and current, and involves dividing the low-pass filtered product of voltage and current signals by the RMS values of the two-signal. It is basically taking the ratio of actual power to apparent power. For low cost implementation, a new technique is devised, which is based on sampling the voltage and current signal at a rate lower than the power line frequency and processing the aliased periodic waveforms, which retain the same phase relationship as the original waveform.

A theoretical analysis for estimating the measurement error is carried out by Pandey [20]. Here the measurement error is computed, as a function of number of quantization bits L and the normalized cutoff frequency γ (= f_c / f_s). It is shown that the ac RMS value of the error is given as $\sigma = 2^{-L}\sqrt{8\gamma/3}$, where γ is the normalized cutoff frequency of low pass filter f_c / f_s. Thus it is possible to have a trade-off between measurement update rate and the sampling rate.

Investigation of technique was done through numerical simulation for the two types of implementations. The results of these investigations are presented in Chapter 4. First implementation involved investigations with sampling rate higher than the power line frequency. The two signals, voltage and current were sampled simultaneously at 900 Sa/s. Here the low pass filter used was IIR Chebychev filter, of 6th

order. Numerical simulation results validated the theoretical analysis. Investigations also involved study of effect of harmonics and power line frequency fluctuation on the dissipation factor measurement. For validating the low sampling rate technique, numerical simulation was carried out with sampling rate of 45 Sa/s. The effect of harmonics and power line frequency fluctuation at lower frequency was studied. The analysis and simulation showed that the two waveforms should be band pass filtered to reduce the errors due to harmonic distortion. No significant increase in the variation was obtained for f_o variation over 48-52 Hz

Further work involved carrying out experimental investigations. First step in experimental investigation involved verifying the result of numerical simulation using a loss angle simulator circuit. Experiment results are presented in Chapter 5. Signal acquisition was done using a multi-functions data acquisition card utilizing half of the input range of 12 bit ADC. Then the input waveforms basically have 11 bit quantization. The acquired data corresponding to voltage and current signals were processed as per the proposed technique [14] to compute the dissipation factor. Processing was done using floating point computations, on the waveforms sampled at the rate of 900 Sa/s as well as on the waveforms with sampling rate decimated to 45 Sa/s. Results obtained in both the cases show excellent linearity in the measurement with ratio error of less than 5% and an offset of 600×10^{-5}.

Later, to validate the online technique under high voltage, an experimental setup was developed. A standard air capacitor with different resistor values connecting series capacitor, were used as test objects with different values of tan δ in the range of 500-5000×10^{-5}. Here the test object was excited with a voltage of 1 kV at power line frequency of 50 Hz. Signal acquisition was carried out at the sampling rate of 900 Sa/s and 11 bit quantization. Acquired data were processed offline using floating-point arithmetic. Signals were band pass filtered before processing for computation of dissipation factor. Measured values of dissipation factor show a very linear relationship with the set values obtained from the Schering bridge. The standard deviation obtained range was $3.7\text{-}6.9\times10^{-5}$ for dissipation factor in the range of $500\text{-}5000\times10^{-5}$. Also processing over a long period did not show variation in the dissipation factor.

Similar investigations were carried out with eight different 1 kV transformer bushings. Results obtained showed a drift in the measured value of dissipation factor with time. There drifts were verified using Schering bridge.

In summary, the proposed technique for online monitoring of tan δ has been validated with the help of numerical simulation, low voltage experimental set-up with a loss angle simulator circuit, and high voltage set-up with test objects at 1 kV.

To make an instrument based on the proposed technique, for high update rate, a floating point DSP processor based board with two-channel 12 bit simultaneous sampling of the signals at 900 Sa/s or higher can be used. However, lower sampling rate can be used to develop a low cost instrument. In lower sampling rate system, the signal acquisition front-end will sample the signals and transmit these acquired signals serially to a central unit for processing. As lower sampling rate has lower update rate, it can be used for monitoring the status of a number of high voltage equipment simultaneously.

Appendix A
FILTER RESPONSES

For low pass filtering in the processing technique of Fig. 1.1 we have experimented with four types of low pass filter, (i) Sixth order IIR Chebychev filter with $\omega_c = 4.44\times10^{-3}\pi$ rad/sa, (ii) Third order IIR Chebychev filter with $\omega_c = 0.06\times10^{-3}\pi$ rad/sa, (iii) FIR Hamming window of order 9000 with $\omega_c = 14.67\times10^{-3}\pi$ rad/sa and (iv) cascade of IIR Chebychev ($\omega_c = 0.62\times10^{-3}\pi$ rad/sa) and FIR Hamming window filter ($\omega_c = 14.67\times10^{-3}\pi$ rad/sa). Further a band pass filter was used to preprocess the current and voltage signal to reduce the dc and harmonics. The filters are tested for their magnitude response by applying an impulse as the input and then magnitude spectrum of the output was found.

A.1 Low pass filter I

First experiments were carried out with IIR Chebychev filter with cut-off frequency of $\omega_c = 4.44\times10^{-3}\pi$ rad/sa. IIR Chebychev filter low pass filter was designed with large attenuation for second harmonic. The designed filter has ripple in the pass band and monotonically increasing attenuation in the stop band. The magnitude and impulse response of this filter are shown in Fig. A.1. To reduce the error due to product term at $2f_o$, we need to have gain at this frequency less than 10^{-8}, i.e. an attenuation of 160 dB. The following specifications were chosen for the filter:

- Pass band ripple < 0.02 dB
- Stop band attenuation of > 200 dB to second harmonic

The filter designed with these specifications has an order of six. The difference equation is given as

$$y(n) = -\sum_{k=1}^{6} a_k y(n-k) + \sum_{k=0}^{6} b_k x(n-k) \qquad \text{(A.1)}$$

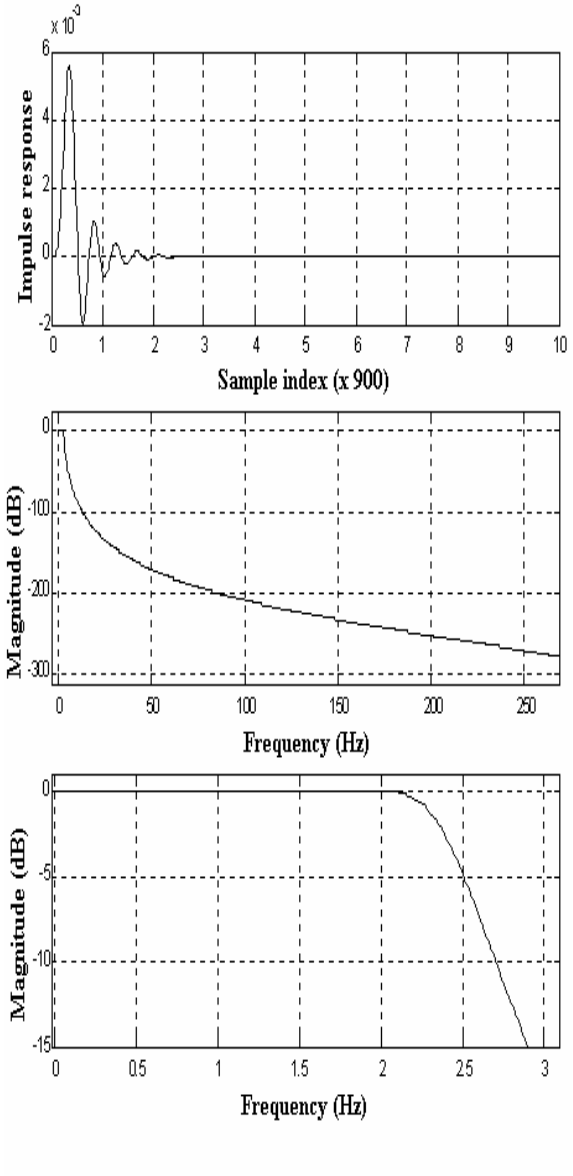

Fig. A.1 Impulse and magnitude responses of IIR Chebychev filter $\omega_c = 4.44\times10^{-3}\pi$ rad/sa. The lower of the two magnitude responses shows a zoomed response in low frequency range.

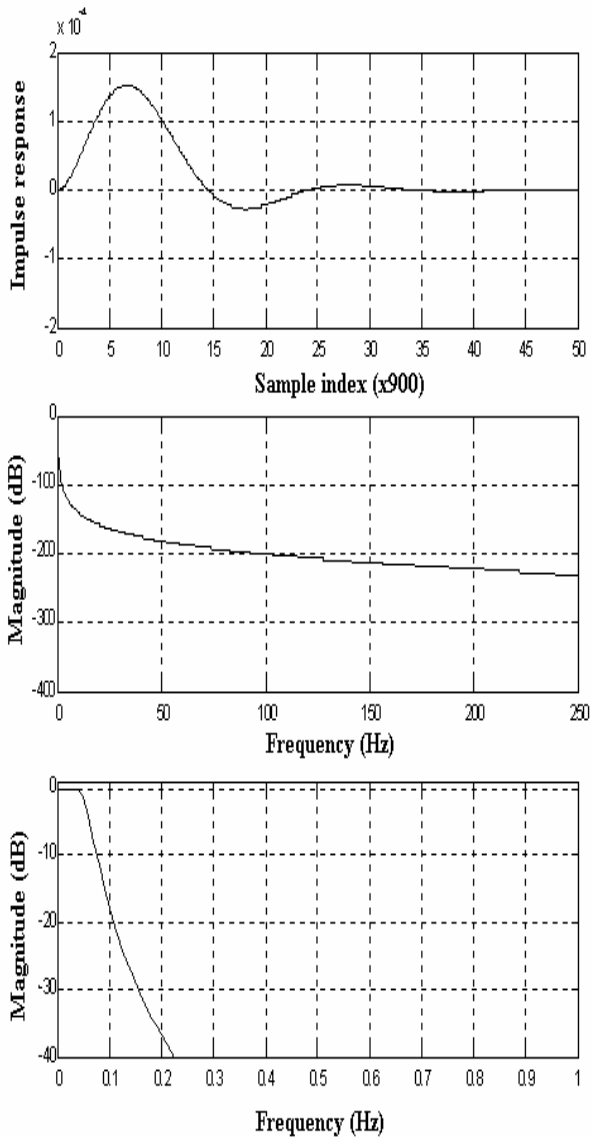

Fig. A.2 Impulse and magnitude responses of IIR Chebychev filter with cut-off of $\omega_c = 0.062\times10^{-3}\pi$ rad/sa. The lower of the two magnitude responses shows a zoomed response in low frequency range.

where, $a_1 = -5.9632$, $a_2 = 14.8170$, $a_3 = -19.6359$, $a_4 = 14.6378$, $a_5 = -5.8199$, $a_6 = 0.9642$, $b_0 = 0.0079 \times 10^{-11}$, $b_1 = 0.0474 \times 10^{-11}$, $b_2 = 0.1201 \times 10^{-11}$, $b_3 = 0.1560 \times 10^{-11}$, $b_4 = 0.1213 \times 10^{-11}$, $b_5 = 0.0468 \times 10^{-11}$, and $b_6 = 0.0081 \times 10^{-11}$

A.2 Low pass filter II

The earlier IIR Chebychev low pass filter was redesigned with a cut-off frequency $\omega_c = 0.062 \times 10^{-3}\pi$ rad/sa. The designed filter was a 3rd order with pass band ripple less than 0.05 dB. Response of this filter is shown in Fig. A.2 and the difference equation is given as

$$y(n) = -\sum_{k=1}^{3} a_k y(n-k) + \sum_{k=0}^{3} b_k x(n-k) \qquad \text{(A.2)}$$

where, $a_1 = -2.9994$, $a_2 = 2.9989$, $a_3 = -0.9994$, $b_0 = 0.04774 \times 10^{-10}$, $b_1 = 0.1433 \times 10^{-10}$, $b_2 = 0.1432 \times 10^{-10}$, $b_3 = 0.0478 \times 10^{-10}$

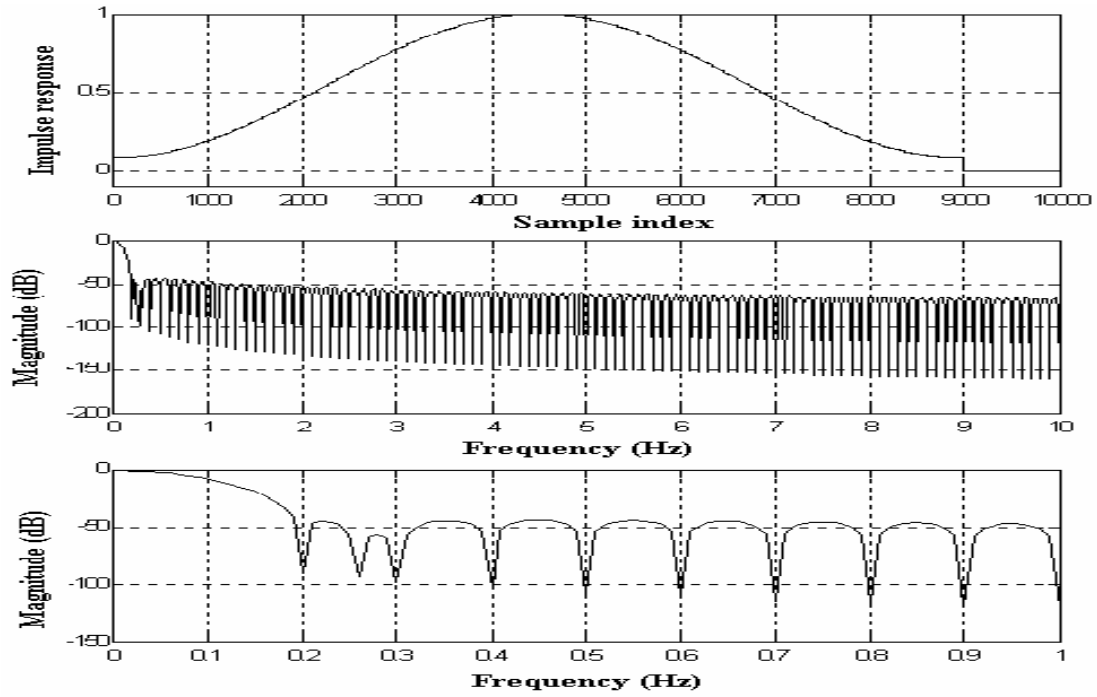

Fig. A.3 Impulse and magnitude responses of FIR Hamming window filter with cut-off $\omega_c = 14.67 \times 10^{-3}\pi$ rad/sa. The lower of the two magnitude responses shows a zoomed response in low frequency range.

A.3 Low pass filter III

Another low pass filter used for experimentation includes FIR Hamming window filter. This filter was designed for order of 9000, with cut-off of $\omega_c = 14.67\times10^{-3}\pi$ rad/sa. The designed filter has an attenuation of -200 dB at notch i.e. 0.2 Hz. Response of this filter is shown in Fig A.3.

A. 4 Band pass filter

The band pass filter was designed as IIR Chebychev filter having ripple in the pass band and monotonically increasing attenuation in stop band. The band pass filter was designed as a 5^{th} order filter to have pass band range of 47-53 Hz with a ripple in pass band less than 0.01 dB. Response of this BPF is shown in Fig A.4

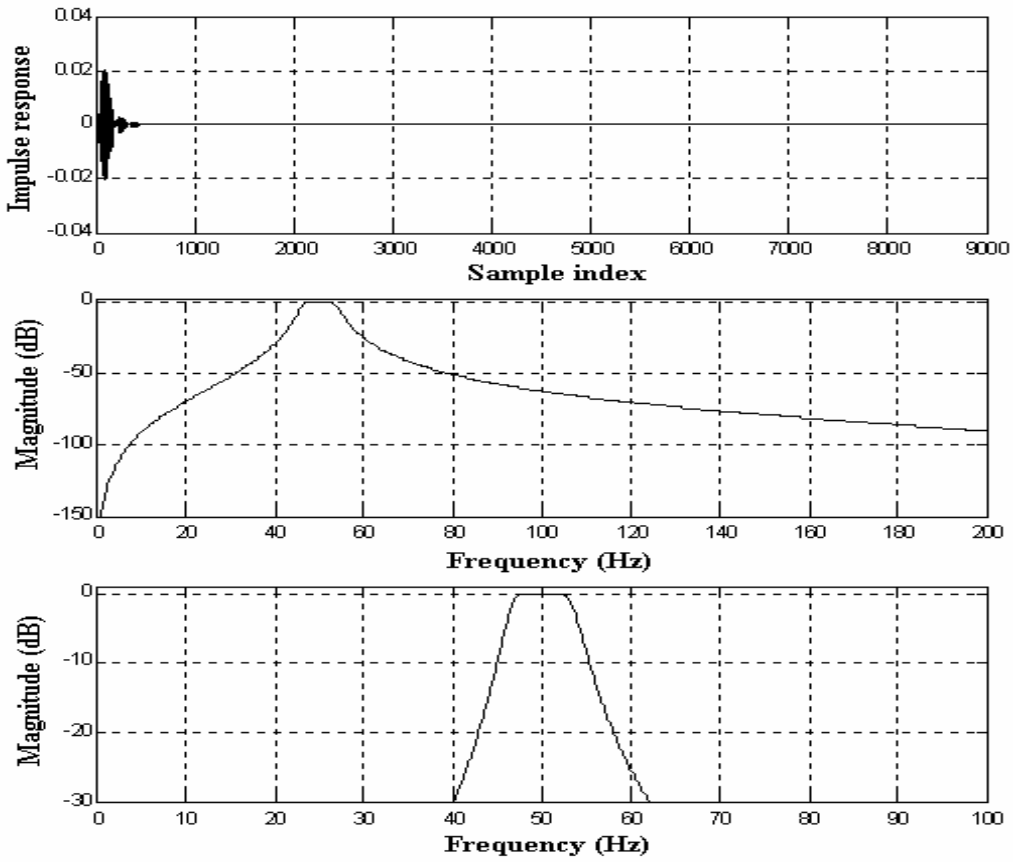

Fig. A.4 Impulse and magnitude responses of IIR Chebychev BPF. The lower of the two magnitude responses shows a zoomed response in low frequency range.

Appendix B
DATA ACQUISITION CARD

The data acquisition card unit USBDAQ-9100MS from M/s Adlink Technology Inc. (Taiwan) was used for signal acquisition. This unit has an isolated interface card with the following features:

- Multi-function data acquisition modules attached to PCs via USB
- 8 differential analog input channels with 12-bit resolution
- Simultaneously sampling of 4 analog input channels (2 sets, totally 8 channels)
- Up to 500 k Sa/s sampling rate
- On board 4 K samples FIFO memory
- 8 isolated digital input and 8 isolated digital output (1500 Vrms)
- Windows driver support

The unit was used with signal acquisition software developed by V. K. Pandey in SPI Lab, EE Dept., IIT Bombay. The program has graphical user interface (GUI) developed in Visual Basic and it uses A/D driver routines for acquisition of the signals. The data are sampled at specified sampling rate and for specified number of samples

REFERENCES

[1] D. Kind, *An Introduction to High Voltage Experimental Technique.* New Delhi, India: Wiley Eastern, 1978.

[2] D. V. Razevig, *High Voltage Engineering*. Delhi, India: Khanna, 1972.

[3] E. W. Golding, *Electrical Measurements and Measuring Instruments*, 4th edition. London, U.K.: Pitman, 1955.

[4] P. Vujovic, R. K. Fricker, J. A. Ehrich, and A. R. Young, "Development of an on-line continuous tan δ monitoring system," in *Proc. IEEE International Symposium on Electrical Insulation*, (Pittsburgh, Pennsylvania), 1994, pp. 50-53.

[5] P. Wang, M. R. Raghuveer, W. McDermid, and J. C. Bromley, "A digital technique for the online measurement of dissipation factor and capacitance," *IEEE Trans. on Dielectrics and Electrical Insulation*, vol.8, no.2, pp. 228-232, April 2001.

[6] N. A. F. Jaeger, G. S. Polovick, H. Kato, and S.E. Cherukapalli, "Online dissipation factor monitoring of high voltage current transformers and bushings," in *Proc. International Council on Large Electric Systems (CIGRE)*, (Paris, New York), Session 1998.

[7] X. Hang, F. Bai, and Z. Yan, "Online measuring dielectric loss angle of capacitive type insulation by using digital measurement technique," in *Proc. IEEE International Symposium on Electrical Insulating Materials*, (Tokyo, Japan), Sept.1995, pp. 275-278.

[8] H. Zhang, K. Tan, F. Dong, and J. Wang, "The analysis of on-line monitored results for capacitive type of equipment," in *Proc. International Symposium on Electrical Insulating Materials (ISEIM)*, (Himeji, Japan), Nov. 2001, pp. 805-808.

[9] B. Djokic, "Phase measurement of distorted periodic signals based on nonsynchronous digital filtering," *IEEE Trans. on Instrumentation and Measurement*, vol.50, no.4, pp. 864-867, Aug. 2001.

[10] S. J. Kearley, "A microcomputer controlled loss angle meter," in *Proc. 5th Int. Conf. on Dielectric Materials, Measurements and Applications*, (Canterbury, UK), June 1998, pp. 194-198.

[11] M. F. Lachman, W. Walter, and P. A. Von Guggenberg, "On-line diagnostics of high-voltage bushings and current transformers using the sum current method," *IEEE Trans. on Power Delivery*, vol.15, no.1, pp. 155-162, Jan. 2000.

[12] R. Brusetti, "Experience with online-diagnostics for bushings and current transfomers," in *Proc. Doble Engineering Neta World Seminar*, Fall 2002, pp. 1-4.

[13] Z. Xiaoming and L. Kaipei, "An active AC bridge with adaptive current orthogonal decomposition for precision measurement of dielectric loss angle," in *Proc. of 2002 Int. Conf. on Precision Electromagnetic Measurements*, June 2002, pp. 182-183.

[14] P. C. Pandey, "Me*asurement of very low tan δ*," unpublished note, EE Dept., IIT Bombay, March 1997, revised November 1997.

[15] S. P. Solanki, "Electronic instrumentation for online monitoring of dissipation factor," M.Tech. Dissertation, Supervisors: P. C. Pandey and S. V. Kulkarni, EE Dept., IIT Bombay, 2003.

[16] V. J. Kumar, P. Sankaran, and K. S. Rao, "Measurement of C and tan δ of a capacitor employing PSDs and dual-slope DVMs," *IEEE Trans. on Instrumentation and Measurement*, vol.52, no.5, pp. 1588-1592, Oct. 2003.

[17] K. M Ibrahim and M. A. H. Abdul Karim, "A novel digital phase meter," *IEEE Trans. Instrumentation and Measurement*, vol-IM-36, pp. 711-716, Sept. 1987.

[18] T. S. Rathore and L. S. Mombasawala, "An accurate digital phase measurement scheme," in *Proc. IEEE*, vol. 72, March 1987, pp. 297-298.

[19] P. K. Hota and N. G. P. C. Mahalik, "A frequency independent ROM-based digital meter for measurement of dissipation factor," in *Proc. 4th Int. Conf. on Properties and Applications of Dielectric Materials*, (Brisbane, Australia), 1994, pp. 690-692.

[20] S. M. Mahmud, A. Rusek, and S. Ganesan, "A microprocessor based dual slope phase meter," *IEEE Trans. Instrumentation & Measurement*, Vol. 37, pp. 374-278, September 1988.

[21] Doble Engineering Company, M4100 Instrument, Watertown, Massachusetts, 2005, http://www.doble.com.

[22] Haefely Test AG, Type 470 bridge, Basel, Switzerland, 2005, http://www.haefely.com.

[23] Megger Group Ltd, Delta2000 Instrument, Mumbai, India, 2005, http://www.avointl.com.

[24] Sivananda Electronics, MLS 11DA1 Instrument, Mumbai, India, 2005, http://www.sivananda electronics.com.

[25] Tinsley Group Ltd, AFP3000 -ITS 12 Instrument, Instrument catalogue, India, 2005.

[26] Presco AG, Type FT12 Instrument, Weiningen, Switzerland, 2005, http://www.prescoag.com.

[27] Eltel Industries Ltd, ACTS-12K Instrument, Bangalore, India, 2005, http://www.eltelindustries.com.

[28] Lemke Diagnostics AG, LDV5/E Instrument, Dresden, Germany, 2005, http://www.ldic.ch.

[29] A. J. Moulson, and J. M. Herbert, *Electroceramics: Materials, Properties Applications*, 2nd edition. London, U.K.: Wiley, 2003.

[30] A. Ambardar, *Analog and Digital Signal Processing*, 2nd edition. Singapore: Thomson Brooks, 2002.

[31] J. G. Proakis and D. G. Manolakis, *Digital Signal Processing*, 3rd edition. New Delhi, India: Prentice Hall, 1999.

[32] A. V. Oppenheim and R. W. Schafer, *Digital Signal Processing*, 2nd edition. New Delhi, India: Prentice Hall, 1994.

[33] S. K. Mitra, *Digital Signal Processing: a Computer-Based Approach.* New Delhi, India: Tata McGraw-Hill, 2001.

[34] T. S. Rathore, *Digital Measurement Technique.* New Delhi, India: Narosa Publishing House, 1996.

[35] Ludeman and Lonnie C, *Fundamentals of Digital Signal Processing*. Chichester: John Wiley, 2003.